Title: Treatment with furosemide indirectly increases inhibitory transmission in the developing hippocampus

Authors: C. Peerboom[1], T. Wijne[1] and C.J. Wierenga[1,2]

Corresponding author: Corette J. Wierenga

Affiliations:

[1] Cell Biology, Neurobiology and Biophysics, Biology department, Utrecht University, 3584 CH, Utrecht, the Netherlands,

[2] Donders Institute for Brain, Cognition and Behaviour, Radboud University, 6525 AJ, Nijmegen, the Netherlands

Author contributions

C.P., and C.J.W. designed research; C.P and T.W., performed research and analyzed data; C.P., and C.J.W. wrote the paper.

Declaration of Interests

The authors declare no competing interests.

Acknowledgements

This research was supported by a TOP grant from ZonMW (#91216021) and by the Nederlandse Organisatie voor Wetenschappelijk Onderzoek (NWO; #OCENW.KLEIN.150). We thank Prof. Thomas Kuner for providing the Cre-dependent SClm construct (Boffi et al., 2018). We thank Prof. Kevin Staley for providing the SuperClomeleon$^{lox/-}$ mouse line, Dr. Stefan Berger for the CamKIIα$^{Cre/-}$ mice and Dr. Henk Karst for sharing these mice with us. We thank Dunya Selemangel for help with SuperClomeleon data analysis and René van Dorland for excellent technical support.

Abstract

During the first two postnatal weeks intraneuronal chloride concentrations in rodents gradually decrease, causing a shift from depolarizing to hyperpolarizing γ-aminobutyric acid (GABA) responses. GABAergic depolarization in the immature brain is crucial for the formation and maturation of excitatory synapses, but when GABAergic signaling becomes inhibitory it no longer promotes synapse formation. Here we examined the role of chloride transporters in developing postnatal hippocampal neurons using furosemide, an inhibitor of the chloride importer NKCC1 and chloride exporter KCC2 with reported anticonvulsant effects. We treated organotypic hippocampal cultures made from 6 to 7-day old mice with 200 µM furosemide from DIV1 to DIV8. Using perforated patch clamp recordings we observed that the GABA reversal potential was depolarized after acute furosemide application, but after a week of furosemide treatment the GABA reversal potential but was more hyperpolarized compared to control. Expression levels of the chloride cotransporters were unaffected after one week furosemide treatment. This suggests that furosemide inhibited KCC2 acutely, while prolonged treatment resulted in (additional) inhibition of NKCC1, but we cannot exclude changes in HCO_3^-. We assessed the effects of accelerating the GABA shift by furosemide treatment on inhibitory synapses onto CA1 pyramidal cells. Directly after cessation of furosemide treatment at DIV9, inhibitory synapses were not affected. However at DIV21, two weeks after ending the treatment, we found that the frequency of inhibitory currents was increased, and VGAT puncta density in *stratum Radiatum* was increased. In addition, cell capacitance of CA1 pyramidal neurons was reduced in furosemide-treated slices at DIV21 in an activity-dependent manner. Our results suggest that furosemide treatment indirectly promoted inhibitory transmission, possibly by increasing activity-independent GABA release.

Introduction

γ-Aminobutyric acid (GABA) is the main inhibitory, hyperpolarizing neurotransmitter in the adult brain, but during early development GABA actually depolarizes neurons. Ionotropic $GABA_A$ receptors primarily conduct chloride (~70%), but also HCO_3^- ions (~30%) (Kaila et al., 2014). While HCO_3^- levels remain constant, intracellular chloride levels decrease during brain development (Kaila et al., 2014). This developmental decrease in chloride causes the reversal potential (E_{GABA}) to gradually drop below resting membrane potential. As a result, the GABAergic driving force shifts from depolarizing in immature neurons to hyperpolarizing in the mature brain (Rivera et al., 1999; Hübner et al., 2001; Tyzio et al., 2007; Romo-Parra et al., 2008; Kirmse et al., 2015; Tsukahara et al., 2015; Sulis Sato et al., 2017; Murata and Colonnese, 2020). The decrease in chloride levels is the direct result of an increased function of the chloride exporter KCC2 (K-Cl cotransporter 2) relative to the chloride importer NKCC1 (Na-K-2Cl cotransporter 1) (Rivera et al., 1999; Gulyás et al., 2001; Yamada et al., 2004; Dzhala et al., 2005; Otsu et al., 2020). In humans, the shift in chloride transporter expression occurs during the first year after birth (Dzhala et al., 2005; Sedmak et al., 2016). In rodents, the GABA shifts during the first two postnatal weeks (Rivera et al., 1999; Stein et al., 2004; Tyzio et al., 2007; Romo-Parra et al., 2008; Kirmse et al., 2015; Sulis Sato et al., 2017; Murata and Colonnese, 2020).

Depolarizing GABA signaling plays a critical role in the formation and maturation of excitatory synapses in the developing brain (Leinekugel et al., 1997; Akerman and Cline, 2006; Wang and Kriegstein, 2008, 2011; Chancey et al., 2013; van Rheede et al., 2015; Oh et al., 2016). However, after the first postnatal week, GABA becomes inhibitory and GABA signaling no longer promotes synapse formation (Salmon et al., 2020; Peerboom et al., 2023). Here we examined the role of chloride transporters in the development of inhibitory synapses in organotypic hippocampal cultures using furosemide, a well-known inhibitor of chloride transport. Treatment with furosemide has been employed previously to block KCC2 and elevate chloride concentrations in (slice) cultures (Thompson and Gahwiler, 1989; Jarolimek et al., 1999; Deeb et al., 2013; Wright et al., 2017), as furosemide has a preference for inhibiting KCC2 over NKCC1 (IC_{50} ~30 µM for rat NKCC1 and IC_{50}~10 µM for rat KCC2, expressed in Xenopus oocytes (Orlov et al., 2015)). In addition, furosemide may interfere with

68 α6- and α4-subunit containing $GABA_A$ receptors (Thompson and Gahwiler, 1989; Pearce,
69 1993; Korpi et al., 1995), and with the regulation of neuronal HCO_3^- levels (Halligan et al.,
70 1991; Temperini et al., 2009; Ruusuvuori and Kaila, 2014; Uwera et al., 2015). Moreover,
71 furosemide was shown to inhibit activity-induced swelling of epileptic brain tissue (Hochman
72 et al., 1995; Gutschmidt et al., 1999; Hochman, 2012).

73

74 We examined the effects of 200 µM furosemide in organotypic hippocampal cultures. We
75 observed that acute furosemide application depolarized GABA reversal potential, in line with
76 a preferential inhibition of KCC2. In contrast, furosemide treatment from DIV1 to DIV8
77 resulted in hyperpolarization of the GABA reversal potential. Expression levels of the chloride-
78 cotransporters were unaffected after furosemide-treatment. This suggests that sustained
79 application of furosemide resulted in inhibition of NKCC1, although we cannot exclude
80 changes in HCO_3^- levels. We assessed the consequences of the accelerated GABA shift during
81 furosemide treatment on inhibitory transmission. We found that inhibitory synapses were
82 not affected directly after furosemide treatment at DIV9. However at DIV21, when E_{GABA} had
83 normalized, inhibitory currents were strongly increased in furosemide-treated slices, possibly
84 via an increased number of inhibitory synapses in the *stratum Radiatum*. In addition, we
85 found evidence for shrinkage of CA1 pyramidal neurons in furosemide-treated slices at DIV21.
86 Our results suggest that furosemide may indirectly promote inhibitory transmission.

87

88 ***Methods***

89 *Animals*

90 All animal experiments were performed in compliance with the guidelines for the welfare of
91 experimental animals issued by the Federal Government of the Netherlands and were
92 approved by the Dutch Central Committee Animal experiments (CCD), project
93 AVD1080020173847 and project AVD1150020184927. In this study we used male and female
94 transgenic mice: GAD65-GFP mice (López-Bendito et al., 2004) (bred as a heterozygous line in
95 a C57BL/6JRj background), C57BL/6JRj littermates, and SuperClomeleon (SClm) mice. The
96 SClm mice (Herstel et al., 2022) are $SuperClomeleon^{lox/-}$ mice (Rahmati et al., 2021), a gift from
97 Kevin Staley (Massachusetts General Hospital, Boston, MA) crossed with $CamKIIα^{Cre/-}$ mice
98 (Tsien et al., 1996; Casanova et al., 2001a). SClm mice express the chloride sensor SClm in up

to 70% of the pyramidal neurons in the hippocampus (Casanova et al., 2001b; Wang et al., 2013). GAD65-GFP mice express GFP in ∼20% of GABAergic interneurons in the CA1 region of the hippocampus (Wierenga et al., 2010). As we did not detect any differences between slices from male and female mice as well as between GAD65-GFP mice and C57BL/6JRj littermates, all data were pooled.

Organotypic hippocampal culture preparation and furosemide-treatment

Organotypic hippocampal cultures were made from P6-7 mice as described before (Hu et al., 2019; Herstel et al., 2022), based on the *Stoppini method* (Stoppini et al., 1991). Mice were decapitated and their brain was rapidly placed in ice-cold Grey's Balanced Salt Solution (GBSS; containing (in mM): 137 NaCl, 5 KCl, 1.5 $CaCl_2$, 1 $MgCl_2$, 0.3 $MgSO_4$, 0.2 KH_2PO_4 and 0.85 Na_2HPO_4) with 25 mM glucose, 12.5 mM HEPES and 1 mM kynurenic acid (pH set at 7.2, osmolarity set at ~320 mOsm, sterile filtered). 400 µm thick transverse hippocampal slices were cut with a McIlwain tissue chopper. Slices were placed on Millicell membrane inserts (Millipore) in wells containing 1 ml culture medium (consisting of 48% MEM, 25% HBSS, 25% horse serum, 25 mM glucose, and 12.5 mM HEPES, with an osmolarity of ~325 mOsm and a pH of 7.3 – 7.4). Slices were stored in an incubator (35°C with 5% CO_2). At DIV1 culture medium was replaced by culture medium supplemented with 0.1% dimethyl sulfoxide (DMSO, Sigma-Aldrich) or 200 µM furosemide (furosemide, Merck, in 0.1 % DMSO). In addition, a small drop of medium supplemented with DMSO or furosemide was carefully placed on top of the slices. In this way, cultures were treated 3 times per week until DIV8. From DIV8 onwards, cultures received normal culture medium 3 times per week. Experiments were performed at day in vitro 1-3 (DIV2), 8-10 (DIV9) or 20-22 (DIV21). Please note that perforated patch experiments at DIV9 were performed 1 to 55 hr after cessation of the furosemide treatment. E_{GABA} did not correlate with hours after treatment and was not affected by addition of furosemide to the ACSF during the perforated patch recording.

Electrophysiology and analysis

Organotypic cultures were transferred to a recording chamber and continuously perfused with carbonated (95% O_2, 5% CO_2) artificial cerebrospinal fluid (ACSF, in mM: 126 NaCl, 3 KCl, 2.5 $CaCl_2$, 1.3 $MgCl_2$, 26 $NaHCO_3$, 1.25 NaH_2PO_4, 20 glucose; with an osmolarity of ~310 mOsm)

130 at a rate of approximately 1 ml/min. Bath temperature was maintained at 29-32°C.
131 Recordings were acquired using an MultiClamp 700B amplifier (Molecular Devices), filtered
132 with a 3 kHz Bessel filter and stored using pClamp10 software. For acute application, ACSF
133 containing 0.1% DMSO or 200 µM furosemide (dissolved in 0.1% DMSO) was bath applied for
134 5 minutes.
135 Perforated patch clamp recordings were performed in CA1 pyramidal neurons. Recording
136 pipettes with resistances of 2-4 MΩ were pulled from borosilicate glass capillaries (World
137 Precision Instruments). The pipette tip was filled with gramicidin-free KCl solution (140 mM
138 KCl and 10 mM HEPES, pH adjusted to 7.2 with KOH, and osmolarity 285 mOsm/l) and then
139 backfilled with solution containing gramicidin (60 µg/ml, Sigma). Neurons were held at -65
140 mV and the access resistance of the perforated cells was monitored constantly before and
141 during recordings by a 5 mV seal test. An access resistance of 50 MΩ was considered
142 acceptable to start recording. Recordings were excluded if the resting membrane potential
143 exceeded -50 mV or if the series resistance after the recording deviated more than 30% from
144 its original value. $GABA_A$ currents were induced by upon local application of 50 µM muscimol
145 dissolved in HEPES-ACSF (containing in mM: 135 NaCl, 3 KCl, 2.5 $CaCl_2$, 1.3 $MgCl_2$, 1.25
146 $Na_2H_2PO_4$, 20 Glucose, and 10 HEPES) every 30 sec using a Picospritzer II (20 ms). Muscimol
147 responses were recorded in the presence of 1 µM TTX (Abcam) at holding potentials between
148 -100 mV and -30 mV in 10 mV steps. We plotted response amplitude as a function of holding
149 potential and calculated the chloride reversal potential from the intersection of the linear
150 current-voltage curve with the x-axis. To assess the size of $GABA_A$ currents independent of
151 holding and reversal potential, we calculated the slope of the current-voltage-plot.
152
153 For recordings of spontaneous inhibitory postsynaptic currents (sIPSCs) and miniature
154 inhibitory currents (mIPSCs) we performed whole-cell patch clamp recordings from CA1
155 pyramidal neurons using borosilicate glass pipettes with resistances of 3-6 MΩ. Pipettes were
156 filled with a KCl-based internal solution (containing in mM: 70 K-gluconate, 70 KCl, 0.5
157 ethyleneglycol- bis(β-aminoethyl)-N,N,N′,N′-tetraacetic Acid (EGTA), 4 Na_2phosphocreatine,
158 4 MgATP, 0.4 NaGTP and 10 HEPES; pH adjusted to 7.2 with KOH) and ACSF was supplemented
159 with 20 µM DNQX (Tocris) and 50 µM DL-APV (Tocris). For recordings of miniature IPSCs
160 (mIPSCs), 1 µM TTX (Abcam) was also added to the ACSF. sIPSCs and mIPSCs were recorded
161 for 6 minutes. For wash in experiments, an sIPSC baseline was recorded for 6 minutes and

compared to sIPSCs after 20 minutes wash in of 1 µM TTX (Abcam), 0.2 µM K252a (Tocris), 5 µM AM251 (Sigma) or 1 µM agatoxin-IVA (smartox-biotech), again for 6 minutes. Membrane capacitance and series resistance were monitored during the recordings by a 5 mV seal test. Cells were discarded if series resistance was above 35 MΩ or if the resting membrane potential exceeded -50 mV or if the series resistance after the recording deviated more than 30% from its original value.

All data were blinded before analysis. Events were selected using a template in Clampfit10 software. Further analysis was performed using custom-written MATLAB scripts. Rise time of sIPSCs was determined as the time between 10% and 90% of the peak value. The decay tau was fitted with a single exponential function. Only events with a goodness of fit $R^2 \geq 0.75$ were included.

Two-photon SuperClomeleon imaging and analysis

We performed two-photon chloride imaging in CA1 pyramidal cells using the SuperClomeleon sensor (Grimley et al., 2013) in cultured slices from SClm mice (Herstel et al., 2022). The SClm sensor consists of Cerulean (a CFP mutant) and Topaz (a YFP mutant) joined by a flexible linker. In the absence of chloride, Fluorescence Resonance Energy Transfer (FRET) occurs from the CFP donor to the YFP acceptor. Chloride binding to YFP increases the distance between the fluorophores and decreases FRET (Grimley et al., 2013).

At the recording day, slices were transferred to a recording chamber and continuously perfused with carbonated (95% O_2, 5% CO_2) ACSF supplemented with 1 mM Trolox, at a rate of approximately 1 ml/min. Bath temperature was monitored and maintained at 30-32 °C. Two-photon imaging of CA1 pyramidal neurons or VGAT-positive interneurons in the CA1 area of the hippocampus was performed using a customized two-photon laser scanning microscope (Femto3D-RC, Femtonics, Budapest, Hungary) with a Ti-Sapphire femtosecond pulsed laser (MaiTai HP, Spectra-Physics) and a 60x water immersion objective (Nikon NIR Apochromat; NA 1.0) The CFP donor was excited at 840 nm. The emission light was split using a dichroic beam splitter at 505 nm and detected using two GaAsP photomultiplier tubes. We collected fluorescence emission of Cerulean/CFP (485 ± 15 nm) and Topaz/YFP (535 ± 15 nm)

193 in parallel. Of each slice from SClm mice, 2-5 image stacks were acquired in different fields of
194 view. The resolution was 8.1 pixels/µm (1024x1024 pixels, 126x126 µm) with 1 µm z-steps.
195
196 Image analysis was performed using ImageJ software, as described before (Herstel et al.,
197 2022). We manually determined regions of interest (ROIs) around individual neuron somata.
198 To select a representative cell population in SClm slices, in each image z-stack we selected
199 four z-planes at comparable depths in which three pyramidal cells were identified that varied
200 in CFP brightness (bright, middle and dark). We subtracted the mean fluorescence intensity
201 of the background in the same image plane before calculating the fluorescence ratio of CFP
202 and YFP. We limited our analysis to cells which were located within 450 pixels from the center
203 of the image, as FRET ratios showed slight aberrations at the edge of our images. We excluded
204 cells with a FRET ratio < 0.5 or > 1.6 to avoid unhealthy cells.
205
206 *Protein extraction and Western Blot analysis*
207 Organotypic hippocampal cultures were washed in cold PBS and subsequently lysed in cold
208 protein extraction buffer containing: 150 mM NaCl, 10 mM EDTA 10 mM HEPES, 1% Triton-
209 X100 and 1x protease and 1x phosphatase inhibitors cocktails (Complete Mini EDTA-free and
210 phosSTOP, Roche). Lysates were cleared of debris by centrifugation (14,000 rpm, 1 min, 4°C)
211 and measured for protein concentration before storage at −20°C until use. Lysates were
212 denatured by adding loading buffer and heating to 95°C for 5 min. For each sample an equal
213 mass of proteins was resolved on 4–15 % polyacrylamide gel (Bio-Rad). The proteins were
214 then transferred (300 mA, 3h) onto ethanol-activated Immobilon-P PVDF membrane
215 (Millipore) before blocking with 3% Bovine Serum Albumin in Tris- buffered saline-Tween
216 (TBST, 20 mM Tris, 150 mM NaCl, 0.1% Tween-20) for 1 h. Primary antibodies used in this
217 study were: mouse anti-NKCC1 (T4, Developmental Studies Hybridoma Bank, 1:1000), rabbit
218 anti-KCC2 (07-432, Merck, 1:1000) and s940-pKCC2 (p1551-940, LuBioSciences, 1:1000),
219 mouse anti-tubulin (T-5168, Sigma, 1:10000). Primary antibodies were diluted in blocking
220 buffer and incubated with the blots overnight at 4 °C under gentle rotation. The membrane
221 was washed 3 times 15 minutes with TBST before a 1h incubation of horseradish peroxidase
222 (HRP)-conjugated antibodies (P0447 goat anti-mouse IgG HRP, Dako, 1:2500 or P0399 swine
223 anti-rabbit IgG HRP, Dako, 1:2500), and washed 3 times 15 minutes in TBST again before
224 chemiluminescence detection. For chemiluminescence detection, blots were incubated with

225 Enhanced luminol-based Chemiluminescence substrate (Promega), and the exposure was
226 captured using the ImageQuant 800 system (Amersham). Images were analyzed in ImageJ, by
227 drawing rectangular boxes around each band and measuring average intensities. Protein
228 levels were normalized to the Tubulin loading controls.
229
230 *Immunohistochemistry, confocal microscopy and analysis*
231 Slices were fixed 4 % paraformaldehyde solution in PBS for 30 minutes at room temperature.
232 After washing slices in phosphate buffered saline (PBS), they were permeabilized for 15
233 minutes in 0.5 % Triton X-100 in PBS for 15 minutes, followed by 1 hour in a blocking solution
234 consisting of 10 % normal goat serum and 0.2 % Triton X-100 in PBS. Slices were incubated in
235 primary antibody solution at 4 °C overnight. The following primary antibodies were used:
236 rabbit polyclonal anti-KCC2 (07-432, Merck, 1:1000), guinea pig anti-NeuN (ABN90, Merck,
237 1:1000), chicken anti-VGAT (131 006, Synaptic Systems, 1:1000), Rabbit anti-PV (PA1-933, Life
238 Technologies, 1:1000), Mouse anti-CB1R (258 011, Synaptic Systems, 1:1000). Slices were
239 washed in PBS and incubated in secondary antibody solution for four hours at room
240 temperature. Secondary antibodies used were goat anti-rabbit Alexa fluor 647 (A21245, Life
241 Technologies, 1:500), goat anti-guinea pig Alexa Fluor 568 (A11075, Life Technologies, 1:500),
242 goat anti-chicken Alexa fluor 647 (A21449, Life technologies, 1:500), goat anti-rabbit Alexa
243 Fluor 405 (A31556, Life Technologies, 1:500), Goat anti-mouse Alexa fluor 488 (A11029, Life
244 Technologies, 1:500). After another PBS wash, slices were mounted in Vectashield mounting
245 medium (Vector labs).
246
247 Confocal images were taken on a Zeiss LSM-700 confocal laser scanning microscopy system
248 with a Plan-Apochromat 40x 1.3 NA immersion objective for KCC2 staining and 63x 1.4 NA oil
249 immersion objective for inhibitory synapse staining. KCC2 staining was imaged in two fields
250 of view in the CA1 *sPyr* of each slice. Inhibitory synapses were imaged in the CA1 *sPyr* and
251 *sRad* of each slice. Image stacks (1024x1024 pixels) were acquired at 6.55 pixels/µm for KCC2
252 staining, 10.08 pixels/µm for VGLUT/VGAT staining. Step size in z was 0.5 µm for KCC2 staining
253 and 0.4 µm for inhibitory synapse staining.
254
255 Confocal images were blinded before analysis. For the analysis of KCC2 levels in control and
256 furosemide-treated slices, ROIs were drawn around 5 NeuN positive cell bodies and this was

257 repeated in 1-3 z-planes (depending on the depth of KCC2 signal) at comparable depths, to
258 measure average KCC2 fluorescence of 5-15 neurons per image stack. For analysis of
259 inhibitory synapses a custom-made macro was used (Ruiter et al., 2020). Briefly, three Z-
260 planes were averaged and background was subtracted with rolling ball radius of 10 pixels.
261 VGAT puncta were identified using watershed segmentation. PV and CB1R channels were
262 thresholded and colocalization with VGAT puncta was analyzed.
263
264 *Statistical Analyses*
265 Statistical analysis was performed in Prism (Graphpad). Normality was tested using the
266 D'Agostino & Pearson test. For the comparison of two groups we either used an unpaired
267 Student's t test (UT; parametric), a Mann-Whitney test (MW; non-parametric), a paired
268 Student's t test (PT; parametric) or a Wilcoxon signed-rank test (WSR; non-parametric). For
269 comparison of multiple groups, a Kruskal Wallis test (KW; nonparametric) was used, followed
270 by a Dunn's Multiple Comparison posthoc test (DMC) or a two way ANOVA (2W ANOVA;
271 parametric), followed by a by a Sidak's Multiple Comparisons posthoc test (SMC). Data are
272 presented as mean ± standard error of the mean. Significance is reported as *$p<0.05$;
273 **$p\leq0.01$; ***$p\leq0.001$.
274
275 ***Results***
276 *Furosemide depolarizes GABA responses acutely, but hyperpolarizes GABA responses after one*
277 *week treatment.*
278 We used perforated patch recordings upon muscimol application in CA1 pyramidal neurons
279 of cultured hippocampal slices to record the reversal potential of $GABA_A$ receptor currents.
280 Acute administration of 200 µM furosemide in DIV2 slices did not affect the GABA reversal
281 potential (E_{GABA}) (Fig. 1A) or GABA driving force (GABA DF) (Fig. 1B), in agreement with a low
282 expression of KCC2 at this age (Salmon et al., 2020; Peerboom et al., 2023). At DIV21, when
283 KCC2 expression is high (Salmon et al., 2020; Peerboom et al., 2023), acute furosemide
284 application elevated E_{GABA} and GABA DF (Fig. 1C,D). This is in agreement with previous reports
285 (Thompson and Gahwiler, 1989; Jarolimek et al., 1999; Deeb et al., 2013; Wright et al., 2017)

286 and comparable with acute inhibition of KCC2 by the specific blocker VU0463271 (VU) in slices
287 at the same developmental stage (Peerboom et al., 2023).

288 We then treated cultured hippocampal slices from DIV1 to DIV8 with 200 µM furosemide.
289 Surprisingly, we observed a strong hyperpolarization of E_{GABA} and a negative shift of the GABA
290 DF at DIV9 after one week of furosemide treatment (Fig. 1E-G). Please note that furosemide
291 was not present during the recordings. Since furosemide has been shown to inhibit α6- and
292 α4-subunit containing $GABA_A$ receptors (Thompson and Gahwiler, 1989; Pearce, 1993; Korpi
293 et al., 1995), we checked if $GABA_A$ receptor inhibition may have interfered with our
294 measurements of E_{GABA} and GABA DF. As a rough indication, we determined the slope of the
295 current-voltage (IV) plot to assess GABA response amplitudes independently of holding
296 potential and reversal potential. However, IV-slopes were not different (MW, p=0.46),
297 suggesting that furosemide did not have a major effect on $GABA_A$ receptors.

298

299 A hyperpolarizing shift in E_{GABA} suggest that furosemide treatment resulted in a reduction of
300 intraneuronal chloride or HCO_3^- levels. To directly assess intracellular chloride levels after
301 furosemide treatment, we employed the chloride sensor SuperClomeleon (SClm) (Grimley et
302 al., 2013; Boffi et al., 2018; Rahmati et al., 2021). We used slices from SClm mice in which CA1
303 pyramidal cells express the SClm sensor and we recorded FRET ratios in control and
304 furosemide-treated slices using two-photon microscopy (Herstel et al., 2022). Remarkably,
305 we did not observe a difference in SClm FRET ratios after one week of furosemide treatment
306 (Fig. 1H,I). The discrepancy between our results from perforated patch recordings and SClm
307 imaging may be due to the decreased sensitivity of the SClm sensor for low chloride levels
308 (Grimley et al., 2013; Herstel et al., 2022). Alternatively, it may reflect concomitant changes
309 in chloride and HCO_3^-, as SClm displays substantial pH-sensitivity (Grimley et al., 2013; Boffi
310 et al., 2018; Lodovichi et al., 2022). These possibilities are discussed in more detail in the
311 discussion section.

312

313 To examine if the hyperpolarizing GABA signaling after furosemide treatment was due to
314 changes in chloride cotransporter expression, we assessed total NKCC1, KCC2 protein levels
315 in control and furosemide-treated slices using Western blots. We also assessed

316 phosphorylated KCC2 at serine 940 (S940-pKCC2), as this phosphorylation regulates KCC2
317 function during development (Lee et al., 2007; Mòdol et al., 2014). No significant changes in
318 the levels of NKCC1, KCC2 or S940-pKCC2 were observed (Fig. 1J,K). In addition, we examined
319 KCC2 localization in treated and control slices using immunohistochemistry. We used NeuN
320 to identify individual cell bodies and we estimated KCC2 levels in somata and membranes. We
321 previously showed that we can detect a reduction in KCC2 levels after shRNA using these
322 methods (Peerboom et al., 2023). Furosemide treatment did not significantly affect KCC2
323 levels in somata or membranes of CA1 pyramidal neurons (Fig. 1L,M). Together, this indicates
324 that furosemide treatment during DIV1 to DIV8 hyperpolarized GABA signaling without
325 changing the expression or surface levels of KCC2, nor by changing expression levels of NKCC1
326 and S940-pKCC2. These results suggest that furosemide treatment hyperpolarized E_{GABA} via
327 inhibition of chloride transporters KCC2 and NKCC1 without altering their expression.

328

329 *Furosemide treatment does not affect inhibitory synapses at DIV9.*

330 The results above show that one week of furosemide treatment resulted in a strong
331 hyperpolarization of E_{GABA}. Next, we assessed the consequences of this altered GABA signaling
332 on inhibitory transmission. We recorded spontaneous and miniature inhibitory currents
333 (sIPSCs and mIPSCs) using whole-cell voltage clamp recordings in CA1 pyramidal cells in
334 control and furosemide-treated slices at DIV9. We found that the frequency and amplitude of
335 sIPSCs were similar in control and furosemide-treated slices at DIV9 (Fig. 2A,B). There were
336 also no differences in rise and decay kinetics and the membrane capacitance (C_m) of CA1
337 pyramidal neurons (Fig. 2C-E). This indicates that GABA signaling does not directly affect the
338 development of inhibitory synapses at this developmental stage (Peerboom et al., 2023).

339

340 When recording sIPSCs, we noticed that the sIPSC frequency slightly increased by ~20% during
341 the first 20 minutes of recording in both control and furosemide-treated slices (Fig. 2F,G),
342 which was associated with a gradual increase of the fraction of sIPSCs with small amplitudes
343 and slow rise times (data not shown). This suggests that the detection of sIPSCs from distal
344 locations gradually improved over time due to diffusion of high chloride internal solution from
345 the recording pipette into the recorded cell. When we washed in TTX, this 'run-up' was

346 compensated by the simultaneous reduction of activity-dependent IPSCs in control slices (Fig.
347 2H). However, in furosemide-treated slices the frequency increase remained during wash-in
348 of TTX (Fig. 2I), suggesting that a smaller fraction of sIPSCs were activity-dependent. We
349 assessed if this difference was due to increased levels of activity-dependent factors that
350 suppress GABA release in furosemide-treated slices, such as endocannabinoids or BDNF. We
351 assessed the contribution of the BDNF receptor TrkB by washing in TrkB antagonist K252a
352 during sIPSC recordings in control and furosemide-treated slices. We found that sIPSC
353 frequency was enhanced after wash-in of K252a, suggesting that there is ongoing suppression
354 of GABA release by BDNF in our slices at DIV9. However, there was no differential contribution
355 of BDNF between control and furosemide-treated slices (Fig. 2J). We also washed in AM251,
356 a specific antagonist of the endocannabinoid receptor CB1. We found that endocannabinoid
357 signaling did not have a prominent influence on sIPSCs, and there was no difference between
358 control and furosemide-treated slices (Fig. 2J). Blocking presynaptic P/Q calcium channels
359 with agatoxin-IVA (aga) (Poncer et al., 1997; Goswami et al., 2012) also did not significantly
360 alter sIPSC frequency in control and furosemide-treated slices (Fig. 2J). These data cannot
361 explain an increase in relative contribution of activity-independent release in sIPSCs after
362 furosemide treatment at DIV9.

363

364 *Inhibitory transmission is increased in furosemide-treated slices at DIV21.*

365 Two weeks after ending the treatment at DIV21, E_{GABA} and GABA DF in pyramidal neurons had
366 normalized and reached control levels (Fig. 3A,B). We previously found that a transient
367 elevation of chloride using VU treatment from DIV1 to DIV8 resulted in indirect changes in
368 inhibitory transmission at DIV21 (Peerboom et al., 2023). We therefore assessed if furosemide
369 treatment from DIV1 to DIV8 affected sIPSCs at DIV21 (Fig. 3C). There was large variability in
370 sIPSC frequency between cells, but we did not detect any significant difference between
371 furosemide-treated and control slices (Fig. 3D). We did observe a small increase in sIPSC
372 amplitude in furosemide-treated slices (Fig. 3E), while the rise and decay time of the sIPSCs
373 were not different (Fig. 3F, G). We noticed that during these sIPSC recordings the cell
374 capacitance C_m of CA1 pyramidal cells gradually decreased in furosemide-treated slices, while
375 C_m values were stable in control slices (Fig. 3H). As resting membrane potential and input

resistance of all recorded cells remained stable, this decrease in C_m appears to be induced by exchange of the cytoplasm of the cells with the high chloride internal solution. We speculate that it may reflect an impaired volume regulation upon chloride load (see discussion). To assess whether the changes in inhibitory transmission were activity-dependent, we also recorded mIPSCs (Fig. 3I). We observed that mIPSCs frequency was increased in furosemide-treated slices at DIV21, while amplitude, rise and decay time were not different from control slices (Fig. 3J-M). For the mIPSC recordings we waited at least 5 minutes before starting the recordings and whole-cell capacitance was stable and not different in control and furosemide-treated slices (Fig. 3N). The observed increase in mIPSC frequency without an accompanying change in sIPSC frequency indicates that activity-independent GABA release was specifically increased in furosemide-treated slices at DIV 21.

A change in mIPSC frequency while the amplitudes remain unaffected could reflect an increase in the number of inhibitory synapses in furosemide-treated slices compared to control slices at DIV21. To assess synapse numbers, we used immunohistochemistry to visualize inhibitory synapses in *stratum Pyramidale (sPyr*) and *stratum Radiatum* (*sRad*) using the vesicular GABA transporter VGAT. In addition, we stained for CB1 receptors (CB1R) and parvalbumin (PV), to identify inhibitory synapses from specific interneuron subtypes (Fig. 4A,B). The density and size of VGAT puncta in the CA1 area were similar in control and furosemide-treated slices at DIV9 (Fig. 4C-F) and we did not observe any differences in the density of CB1R+ and PV+ VGAT puncta (Fig. 4G-I). At DIV21 however (Fig. 5A,B), we observed an increased density and reduced size of VGAT puncta in the *sRad* in furosemide-treated slices compared to controls (Fig. 5E,F), but not in the *sPyr* (Fig. 5C,D). The density of PV- and CB1R-positive puncta were not different in furosemide-treated and control slices (Fig. 5G-I), suggesting that the increase in VGAT puncta is due to synapses from other interneuron subtypes. To assess possible changes in cell size, we analyzed soma area from the NeuN staining, but we found no differences between furosemide-treated and control slices (control: 211 ± 7 μm^2 and furosemide: 211 ± 13 μm^2; p=0.9757, UT-test; 14-16 images from 7-8 slices from 3 mice). These results suggest that the density of inhibitory synapses in the dendritic region was increased at DIV21 in furosemide-treated slices.

406 ***Discussion***

407 In this study, we used furosemide to manipulate the GABA shift in organotypic hippocampal
408 slices. Unexpectedly, we observed that treatment with furosemide from DIV1 to DIV8 had an
409 opposite effect compared to acute furosemide application. While acute application
410 depolarized the reversal potential for GABA signaling (E_{GABA}), one week furosemide treatment
411 resulted in a strong hyperpolarizing shift of E_{GABA}. This shift was not accompanied by a change
412 in SuperClomeleon FRET ratios or chloride co-transporter expression. We observed that
413 sIPSCs were not affected by the hyperpolarization of E_{GABA} after furosemide treatment at
414 DIV9, consistent with the notion that GABA signaling in the second postnatal week no longer
415 promotes synapse formation (Wang and Kriegstein, 2011; Salmon et al., 2020; Peerboom et
416 al., 2023). However, we found that at DIV21, two weeks after ending furosemide treatment
417 and when E_{GABA} had normalized, inhibitory currents were increased. This was accompanied
418 by an increase of the density of VGAT puncta in *sRad*. Together, these results show that
419 accelerating the GABA shift with furosemide does not directly affect the development of
420 inhibitory synapses. However, transient furosemide treatment appeared to indirectly alter
421 increase inhibitory transmission two weeks later. Unfortunately, our data do not provide a
422 clear mechanism explaining these observations, but we offer our thoughts and speculations
423 below.

424

425 *Effect of furosemide on neuronal chloride levels*

426 The depolarizing effect of acute furosemide application at DIV21 was comparable to the
427 depolarization after acute inhibition of KCC2 by specific KCC2 blocker VU0463271 (VU) in
428 slices at the same developmental stage (Peerboom et al., 2023), suggesting that acutely
429 applied furosemide mainly inhibits KCC2. At the concentration used here (200 µM),
430 furosemide is expected to block both KCC2 and NKCC1 (Orlov et al., 2015). However, NKCC1
431 is mainly inactive in adult tissue and maintains chloride levels only until approximately P15-
432 21 (Romo-Parra et al., 2008; Sulis Sato et al., 2017; Salmon et al., 2020). Previous studies also
433 reported a depolarizing effect of furosemide when acutely applied to (slice) cultures at a
434 developmental stage equal to P14 or later (Thompson and Gahwiler, 1989; Jarolimek et al.,
435 1999; Deeb et al., 2013; Wright et al., 2017). In our slices at DIV21 (prepared from P7 mice),

436 NKCC1 may therefore no longer directly regulate chloride levels, which explains why acute
437 furosemide application only acted via KCC2 at DIV21.

438 In stark contrast, furosemide treatment from DIV1 to DIV8 resulted in hyperpolarizing E_{GABA}.
439 As furosemide blocks both main chloride transporters KCC2 and NKCC1, we had predicted
440 that intracellular chloride levels would roughly follow the Nernst equilibrium. The observed
441 hyperpolarized E_{GABA} suggests that an additional chloride extrusion mechanism exists that
442 remains unidentified here. We checked that furosemide treatment did not affect expression
443 levels of chloride transporters. If furosemide treatment hyperpolarized E_{GABA} by reducing
444 intracellular chloride levels, we would expect to observe an increase in SClm FRET ratios
445 (reflecting a decrease in chloride levels) after furosemide treatment, which was not the case.
446 However, although the SClm sensor is useful to detect increases in chloride levels (Peerboom
447 et al., 2023), its sensitivity of is reduced at chloride concentrations below ~5 mM (Grimley et
448 al., 2013), which is close to physiological chloride levels in neurons (Boffi et al., 2018). This
449 suggests that chloride levels in our DIV9 slices after furosemide treatment are too low to
450 detect a further decrease with the SClm sensor.

451

452 *Possible effect of furosemide on pH*

453 In addition to blocking chloride transporters, furosemide may interfere with enzymes that are
454 involved in HCO_3^- regulation (Halligan et al., 1991; Temperini et al., 2009; Uwera et al., 2015).
455 $GABA_A$ receptors are permeable for chloride and HCO_3^- ions with a permeability of around
456 70% and 30% respectively (Kaila et al., 2014). The reversal potential of HCO_3^- is maintained
457 by pH-regulatory proteins at around -10 mV (Kaila et al., 2014), which is much more positive
458 than the chloride reversal potential E_{Cl}). As a result, E_{GABA} is slightly more positive than E_{Cl} and
459 the flow of chloride through $GABA_A$ receptors is accompanied by an outflow of HCO_3^- (Kaila
460 et al., 2014). The lack of change in SClm FRET ratios after furosemide treatment raises the
461 possibility that the observed hyperpolarization of E_{GABA} reflect changes in intracellular HCO_3^-
462 levels, rather than chloride. If furosemide would decrease intraneuronal HCO_3^- levels, the
463 outflow of HCO_3^- upon $GABA_A$ receptor activation would be reduced, and E_{GABA} would become
464 more negative. Previous studies have suggested that furosemide can inhibit the Cl^-/HCO_3^-
465 anion exchanger AE3 (Halligan et al., 1991; Uwera et al., 2015). AE3 exchanges intracellular

466 HCO_3^- for extracellular chloride, thereby lowering intracellular pH and increasing intracellular
467 chloride concentrations in response to intracellular alkali loads (Gonzalez-Islas et al., 2009;
468 Pfeffer et al., 2009; Romero et al., 2013). Furosemide can also block carbonic anhydrase (CA)
469 (Temperini et al., 2009), which is a cytosolic enzyme that mediates the conversion of HCO_3^-
470 ($CO_2 + H_2O \rightleftarrows HCO_3^- + H^+$) to buffer intraneuronal pH after alkali or acid loads (Ruusuvuori and
471 Kaila, 2014). To our knowledge there are no studies directly examining the contribution of
472 AE3 or CA to E_{GABA}. Theoretically, inhibition of AE3 by furosemide would decrease intracellular
473 chloride levels while increasing HCO_3^-, which have opposing effects on E_{GABA}. Inhibition of CA
474 would in theory reduce the contribution of E_{HCO3} to E_{GABA} and result in a negative shift of E_{GABA}
475 towards E_{Cl}. If the hyperpolarization of E_{GABA} that we observed in our experiments were solely
476 due to changing HCO_3^- levels without changing chloride, pH values would be unphysiologically
477 low. As neurons were generally healthy after furosemide treatment, such a large pH change
478 seems unlikely. However, a small reduction in intracellular pH would decrease SClm FRET
479 ratios (Grimley et al., 2013; Boffi et al., 2018; Lodovichi et al., 2022), which may have obscured
480 an increase in FRET ratios due to a decrease in chloride levels. We therefore conclude that
481 furosemide treatment most likely resulted in a decrease in chloride levels, but our data do
482 not exclude an accompanying subtle change in pH regulation.

483

484 *Possible effect of furosemide on cell volume regulation*

485 We observed that the membrane capacitance of CA1 pyramidal neurons gradually reduced
486 after break-in for whole-cell recordings in furosemide-treated slices, but not in control slices
487 at DIV21 (Fig. 3H), and also not at DIV9 (Fig. 2E). A reduction in whole cell membrane
488 capacitance may reflect a reduction in cell size (Taylor, 2012). Previous studies have shown
489 that furosemide inhibits activity-induced changes in the volume of neuronal tissue during
490 epilepsy (Hochman et al., 1995; Gutschmidt et al., 1999) via inhibition of NKCC1 on glia cells
491 (Ransom et al., 1985; Hochman, 2012). Glia disperse local, activity-induced elevations in
492 potassium and chloride ions which are followed by water and result in glial swelling. As
493 capacitance was not different immediately after break-through, cell volume did not appear to
494 be affected per se. This was also supported by the observation that soma sizes of CA1
495 pyramidal cells were found similar in furosemide-treated and control slices. Overall cellular

496 health was not affected in furosemide-treated slices at DIV21 as resting membrane potential
497 and input resistance remained stable during the recordings and were comparable to control
498 slices. Instead, the observed gradual decrease in whole cell capacitance may indicate a loss of
499 cell volume regulation in response to wash-in of the high chloride pipette solution. We
500 speculate that chloride extrusion mechanisms triggered by the high chloride load (Jarolimek
501 et al., 1999) may have instigated loss of cell volume, resulting in the observed C_m decrease.
502 This suggests that the transient furosemide treatment between DIV1 and DIV8 led to long-
503 lasting alterations in chloride homeostasis and/or cell volume regulation.

504

505 *Furosemide-treatment indirectly increased inhibitory transmission*

506 We observed that sIPSCs were not affected by the hyperpolarization of E_{GABA} at DIV9,
507 immediately after the furosemide treatment (Fig. 2A-E). These results confirm previous
508 studies reporting that synapse formation is mostly independent from GABA signaling after the
509 first postnatal week (Wang and Kriegstein, 2011; Peerboom et al., 2023). More surprisingly,
510 we found that furosemide treatment resulted in an increase in inhibitory transmission at
511 DIV21. The frequency of mIPSCs were strongly increased, while sIPSC frequency was less
512 affected. This points to a relative increase in activity-independent GABA release at DIV21,
513 which was also noticeable, although much less pronounced, at DIV9. This may indicate subtle
514 alterations in inhibitory synapses, but we did not further examine release properties. The
515 observed increase in sIPSC amplitude may reflect a compensatory change. In our
516 immunohistochemistry experiments we observed an increased density of inhibitory synapses
517 in *sRad* in furosemide-treated slices compared to control slices, which may explain the
518 increase in mIPSC frequency. However, one should be cautious in interpreting synaptic
519 density in the two conditions, as furosemide treatment may have induced tissue shrinkage
520 (see above), which would increase apparent synaptic density. To determine synaptic densities
521 independently of tissue shrinkage, the density of synapses along the dendrites (Feng et al.,
522 2021) or per soma (Bijlsma et al., 2022) should be assessed.

523

524 *Possible anti-epileptic actions of furosemide*

525 Furosemide is commonly used as a diuretic, but has important anti-epileptic actions. A case-
526 control study on hypertension and epilepsy showed that diuretics including furosemide
527 protected patients with hypertension against an increased risk on seizures in later life
528 (Hesdorffer et al., 1996). Subsequently, the antiepileptic effects of furosemide were
529 demonstrated in several animal models (Hochman et al., 1995; Gutschmidt et al., 1999;
530 Holtkamp et al., 2003; Barbaro et al., 2004; Viitanen et al., 2010; Hochman, 2012; Uwera et
531 al., 2015; Chen et al., 2022). Since then, several epidemiological and experimental studies
532 have reported anticonvulsant actions of furosemide, but because it broad range of activity
533 the mechanism behind furosemide's anti-epileptic effects remains mostly unclear (Hesdorffer
534 et al., 1996; Staley, 2002; Maa et al., 2011). Although the precise mechanism remains obscure,
535 our results suggest that furosemide treatment indirectly increases inhibitory transmission,
536 which adds to its previously described anticonvulsant action. An increase in activity-
537 independent GABA release may result in an increase in ambient GABA levels, mediating a
538 cellular hyperpolarization and reducing overall excitability.

539

540 *Final remarks*

541 In a recent study we treated slice cultures with VU, a specific blocker of the chloride exporter
542 KCC2, to delay the postnatal GABA shift and maintain a depolarizing E_{GABA} until DIV8. Similar
543 to the current results, we also observed an indirect increase in sIPSC frequency at DIV21 cells
544 (Peerboom et al., 2023). However, the mechanism seems different as mIPSC frequency and
545 synapse numbers were not affected in VU-treated slices (Peerboom et al., 2023). In
546 interpreting our results and that of previous studies, it is hard to disentangle the versatile
547 pharmacological profile of furosemide and the many roles for neuronal chloride in regulating
548 cell volume (Jentsch and Pusch, 2018) and possibly cellular excitability (Huang et al., 2012;
549 Seja et al., 2012; Jentsch and Pusch, 2018; Goutierre et al., 2019; Sinha et al., 2022; Peerboom
550 et al., 2023). Our study further underscores the need for a better understanding of the role
551 of chloride as an intracellular messenger in developing neurons.

552

553 ## *References*

554 Akerman CJ, Cline HT (2006) Depolarizing GABAergic conductances regulate the balance of excitation to inhibition in the
555 developing retinotectal circuit in vivo. J Neurosci 26:5117–5130.

556 Barbaro NM, Takahashi DK, Baraban SC (2004) A potential role for astrocytes in mediating the antiepileptic actions of
557 furosemide in vitro. Neuroscience 128:655–663.

558 Bijlsma A, Omrani A, Spoelder M, Verharen JPH, Bauer L, Cornelis C, de Zwart B, van Dorland R, Vanderschuren LJMJ,
559 Wierenga CJ (2022) Social Play Behavior Is Critical for the Development of Prefrontal Inhibitory Synapses and
560 Cognitive Flexibility in Rats. J Neurosci 42:8716–8728.

561 Boffi JC, Knabbe J, Kaiser M, Kuner T (2018) KCC2-dependent steady-state intracellular chloride concentration and ph in
562 cortical layer 2/3 neurons of anesthetized and awake mice. Front Cell Neurosci 12:1–14.

563 Casanova E, Fehsenfeld S, Mantamadiotis T, Lemberger T, Greiner E, Stewart AF, Schtz G (2001a) A CamKIIα iCre BAC allows
564 brain-specific gene inactivation. Genesis 31:37–42.

565 Casanova E, Fehsenfeld S, Mantamadiotis T, Lemberger T, Greiner E, Stewart AF, Schtz G (2001b) A CamKIIα iCre BAC allows
566 brain-specific gene inactivation. Genesis 31:37–42.

567 Chancey JH, Adlaf EW, Sapp MC, Pugh PC, Wadiche JI, Overstreet-Wadiche LS (2013) GABA Depolarization Is Required for
568 Experience-Dependent Synapse Unsilencing in Adult-Born Neurons. J Neurosci 33:6614–6622.

569 Chen L, Yu J, Wan L, Wu Z, Wang G, Hu Z, Ren L, Zhou J, Qian B, Zhao X, Zhang J, Liu X (2022) Furosemide prevents
570 membrane KCC2 downregulation during convulsant stimulation in the hippocampus. IBRO Neurosci Rep 12:355–
571 365.

572 Deeb TZ, Nakamura Y, Frost GD, Davies PA, Moss SJ (2013) Disrupted Cl-homeostasis contributes to reductions in the
573 inhibitory efficacy of diazepam during hyperexcited states. Eur J Neurosci 38:2453–2467.

574 Dzhala VI, Talos DM, Sdrulla DA, Brumback AC, Mathews GC, Benke TA, Delpire E, Jensen FE, Staley KJ (2005) NKCC1
575 transporter facilitates seizures in the developing brain. Nat Med 11:1205–1213.

576 Feng T, Alicea C, Pham V, Kirk A, Pieraut S (2021) Experience-dependent inhibitory plasticity is mediated by CCK1 basket
577 cells in the developing dentate gyrus. J Neurosci 41:4607–4619.

578 Gonzalez-Islas C, Chub N, Wenner P (2009) NKCC1 and AE3 appear to accumulate chloride in embryonic motoneurons. J
579 Neurophysiol 101:507–518.

580 Goswami SP, Bucurenciu I, Jonas P (2012) Miniature IPSCs in hippocampal granule cells are triggered by voltage-gated Ca2+
581 channels via microdomain coupling. J Neurosci 32:14294–14304.

582 Goutierre M, Al Awabdh S, Donneger F, François E, Gomez-Dominguez D, Irinopoulou T, Menendez de la Prida L, Poncer JC
583 (2019) KCC2 Regulates Neuronal Excitability and Hippocampal Activity via Interaction with Task-3 Channels. Cell
584 Rep 28:91–103.

585 Grimley JS, Li L, Wang W, Wen L, Beese LS, Hellinga HW, Augustine GJ (2013) Visualization of Synaptic Inhibition with an
586 Optogenetic Sensor Developed by Cell-Free Protein Engineering Automation. J Neurosci 33:16297–16309.

587 Gulyás AI, Sík A, Payne JA, Kaila K, Freund TF (2001) The KCl cotransporter, KCC2, is highly expressed in the vicinity of
588 excitatory synapses in the rat hippocampus. Eur J Neurosci 13:2205–2217.

589 Gutschmidt KU, Stenkamp K, Buchheim K, Heinemann U, Meierkord H (1999) Anticonvulsant actions of furosemide in vitro.
590 Neuroscience 91:1471–1481.

591 Halligan RD, Shelat H, Kahn AM (1991) Na+-independent Cl--HCO : exchange in sarcolemmal vesicles from vascular smooth
592 muscle. Am J Physiol 260:C347-54.

593 Herstel LJ, Peerboom C, Uijtewaal S, Selemangel D, Karst H, Wierenga CJ (2022) Using SuperClomeleon to measure changes
594 in intracellular chloride during development and after early life stress. Eneuro November/D.

595 Hesdorffer DC, Hauser WA, Annegers JF, Rocca WA (1996) Severe, uncontrolled hypertension and adult-onset seizures: A
596 case- control study in Rochester, Minnesota. Epilepsia 37:736–741.

597 Hochman DW (2012) The extracellular space and epileptic activity in the adult brain: Explaining the antiepileptic effects of
598 furosemide and bumetanide. Epilepsia 53:18–25.

599 Hochman DW, Baraban SC, Owens JWM, Schwartzkroin PA (1995) Dissociation of synchronization and excitability in
600 furosemide blockade of epileptiform activity. Science 270:99–102.

601 Holtkamp M, Matzen J, Buchheim K, Walker MC, Meierkord H (2003) Furosemide terminates limbic status epilepticus in
602 freely moving rats. Epilepsia 44:1141–1144.

603 Hu HY, Kruijssen DLH, Frias CP, Rózsa B, Hoogenraad CC, Wierenga CJ (2019) Endocannabinoid Signaling Mediates Local
604 Dendritic Coordination between Excitatory and Inhibitory Synapses. Cell Rep 27:666-675.e5.

605 Huang WC, Xiao S, Huang F, Harfe BD, Jan YN, Jan LY (2012) Calcium-Activated Chloride Channels (CaCCs) Regulate Action
606 Potential and Synaptic Response in Hippocampal Neurons. Neuron 74:179–192.

607 Hübner C a, Stein V, Hermans-Borgmeyer I, Meyer T, Ballanyi K, Jentsch TJ (2001) Disruption of KCC2 reveals an essential
608 role of K-Cl cotransport already in early synaptic inhibition. Neuron 30:515–524.

609 Jarolimek W, Lewen A, Misgeld U (1999) A furosemide-sensitive K+ -Cl- cotransporter counteracts intracellular Cl-
610 accumulation and depletion in cultured rat midbrain neurons. J Neurosci 19:4695–4704.

611 Jentsch TJ, Pusch M (2018) CLC chloride channels and transporters: Structure, function, physiology, and disease. Physiol
612 Rev 98:1493–1590.

613 Kaila K, Price TJ, Payne JA, Puskarjov M, Voipio J (2014) Cation-chloride cotransporters in neuronal development, plasticity
614 and disease. Nat Rev Neurosci 15:637–654.

615 Kirmse K, Kummer M, Kovalchuk Y, Witte OW, Garaschuk O, Holthoff K (2015) GABA depolarizes immature neurons and
616 inhibits network activity in the neonatal neocortex in vivo. Nat Commun 6:1–13.

617 Korpi ER, Kuner T, Seeburg PH, Luddens H (1995) Selective antagonist for the cerebellar granule cell-specific g-aminobutyric
618 acid type A receptor. MolPharmacol 47:283–289.

619 Leinekugel X, Medina I, Khalilov I, Ben Ari Y, Khazipov R (1997) Ca 2+ Oscillations Mediated by the Synergistic Excitatory
620 Actions of GABA. Neuron 18:243–255.

621 Lodovichi C, Ratto GM, Trevelyan AJ, Arosio D (2022) Genetically encoded sensors for Chloride concentration. J Neurosci
622 Methods 368:109455.

623 Maa EH, Kahle KT, Walcott BP, Spitz MC, Staley KJ (2011) Diuretics and epilepsy: Will the past and present meet? Epilepsia
624 52:1559–1569.

625 Murata Y, Colonnese MT (2020) GABAergic interneurons excite neonatal hippocampus in vivo. Sci Adv 6:1–10.

626 Oh WC, Lutzu S, Castillo PE, Kwon HB (2016) De novo synaptogenesis induced by GABA in the developing mouse cortex -
627 supplemental. Science 353:1037–1040.

628 Orlov SN, Koltsova S V, Kapilevich L V, Gusakova S V, Dulin NO (2015) NKCC1 and NKCC2: The pathogenetic role of cation-
629 chloride cotransporters in hypertension. 2:186–196.

630 Otsu Y, Donneger F, Schwartz EJ, Poncer JC (2020) Cation–chloride cotransporters and the polarity of GABA signalling in
631 mouse hippocampal parvalbumin interneurons. J Physiol 598:1–16.

632 Pearce RA (1993) Physiological evidence for two distinct GABAA responses in rat hippocampus. Neuron 10:189–200.

633 Peerboom C, De Kater S, Jonker N, Rieter MPJM, Wijne T, Wierenga CJ (2023) Delaying the GABA Shift Indirectly Affects
634 Membrane Properties in the Developing Hippocampus. J Neurosci 43:5483–5500.

635 Pfeffer CK, Stein V, Keating DJ, Maier H, Rinke I, Rudhard Y, Hentschke M, Rune GM, Jentsch TJ, Hubner CA (2009) NKCC1-
636 Dependent GABAergic Excitation Drives Synaptic Network Maturation during Early Hippocampal Development. J
637 Neurosci 29:3419–3430.

638 Poncer J-C, Mckinney RA, Thompson SM, Forel-strasse A (1997) Either N- or P-type calcium channels mediate GABA release
639 at distinct hippocampal inhibitory synapses. Neuron 18:463–472.

640 Rahmati N, Normoyle KP, Glykys J, Dzhala VI, Lillis KP, Kahle KT, Raiyyani R, Jacob T, Staley KJ (2021) Unique actions of gaba
641 arising from cytoplasmic chloride microdomains. J Neurosci 41:4967–4975.

642 Ransom B, Yamate C, Connors B (1985) Activity-dependent in rat optic nerve: a developmental study. J Neurosci 5:532–
643 535.

644 Rivera C, Voipio J, Payne J a, Ruusuvuori E, Lahtinen H, Lamsa K, Pirvola U, Saarma M, Kaila K (1999) The K+/Cl- co-
645 transporter KCC2 renders GABA hyperpolarizing during neuronal maturation. Nature 397:251–255.

646 Romero MF, Chen AP, Parker MD, Boron WF (2013) The SLC4 family of bicarbonate (HCO3-) transporters. Mol Aspects Med
647 34:159–182.

648 Romo-Parra H, Treviño M, Heinemann U, Gutiérrez R (2008) GABA actions in hippocampal area CA3 during postnatal
649 development: Differential shift from depolarizing to hyperpolarizing in somatic and dendritic compartments. J
650 Neurophysiol 99:1523–1534.

651 Ruiter M, Herstel LJ, Wierenga CJ, Ma T (2020) Reduction of Dendritic Inhibition in CA1 Pyramidal Neurons in Amyloidosis
652 Models of Early Alzheimer's Disease. J Alzheimers Dis 78:951–964.

653 Ruusuvuori E, Kaila K (2014) Carbonic Anhydrases and Brain pH in the Control of Neuronal Excitability. In: Carbonic
654 Anhydrase: Mechanism, Regulation, Links to Disease, and Industrial Applications, pp 271–290 Subcellular
655 Biochemistry. Springer International Publishing. Available at: https://doi.org/10.1007/978-94-007-7359-2_14.

656 Salmon CK, Pribiag H, Gizowski C, Farmer WT, Cameron S, Jones E V., Mahadevan V, Bourque CW, Stellwagen D, Woodin
657 MA, Murai KK (2020) Depolarizing GABA Transmission Restrains Activity-Dependent Glutamatergic Synapse
658 Formation in the Developing Hippocampal Circuit. Front Cell Neurosci 14:1–16.

659 Sedmak G, Puskarjov NJ-MM, Ulamec M, Krušlin B, Kaila K, Judaš M (2016) Developmental Expression Patterns of KCC2 and
660 Functionally Associated Molecules in the Human Brain. Cereb Cortex 27:4060–4072.

661 Seja P, Schonewille M, Spitzmaul G, Badura A, Klein I, Rudhard Y, Wisden W, Hübner CA, De Zeeuw CI, Jentsch TJ (2012)
662 Raising cytosolic Cl - in cerebellar granule cells affects their excitability and vestibulo-ocular learning. EMBO J
663 31:1217–1230.

664 Sinha AS, Wang T, Watanabe M, Hosoi Y, Sohara E, Akita T, Uchida S, Fukuda A (2022) WNK3 kinase maintains neuronal
665 excitability by reducing inwardly rectifying K+ conductance in layer V pyramidal neurons of mouse medial
666 prefrontal cortex. Front Mol Neurosci 15.

667 Staley KJ (2002) Diuretics as Antiepileptic Drugs: Should We Go with the Flow? Epilepsy Curr 2:39–40.

668 Stein V, Hermans-Borgmeyer I, Jentsch TJ, Hübner CA (2004) Expression of the KCl Cotransporter KCC2 Parallels Neuronal
669 Maturation and the Emergence of Low Intracellular Chloride. J Comp Neurol 468:57–64.

670 Stoppini L, Buchs PA, Muller D (1991) A simple method for organotypic cultures of nervous tissue. J Neurosci Methods
671 37:173–182.

672 Sulis Sato S, Artoni P, Landi S, Cozzolino O, Parra R, Pracucci E, Trovato F, Szczurkowska J, Luin S, Arosio D, Beltram F,
673 Cancedda L, Kaila K, Ratto GM (2017) Simultaneous two-photon imaging of intracellular chloride concentration
674 and pH in mouse pyramidal neurons in vivo. Proc Natl Acad Sci 114:E8770–E8779.

675 Taylor AL (2012) What we talk about when we talk about capacitance measured with the voltage-clamp step method. J
676 Comput Neurosci 32:167–175.

677 Temperini C, Cecchi A, Scozzafava A, Supuran CT (2009) Carbonic anhydrase inhibitors. Comparison of chlorthalidone,
678 indapamide, trichloromethiazide, and furosemide X-ray crystal structures in adducts with isozyme II, when
679 several water molecules make the difference. Bioorg Med Chem 17:1214–1221.

680 Thompson SM, Gahwiler BH (1989) Activity-dependent disinhibition. II. Effects of extracellular potassium, furosemide, and
681 membrane potential on E(Cl)- in hippocampal CA3 neurons. J Neurophysiol 61:512–523.

682 Tsien JZ, Chen DF, Gerber D, Tom C, Mercer EH, Anderson DJ, Mayford M, Kandel ER, Tonegawa S (1996) Subregion- and
683 cell type-restricted gene knockout in mouse brain. Cell 87:1317–1326.

684 Tsukahara T, Masuhara M, Iwai H, Sonomura T, Sato T (2015) Repeated stress-induced expression pattern alterations of the
685 hippocampal chloride transporters KCC2 and NKCC1 associated with behavioral abnormalities in female mice.
686 Biochem Biophys Res Commun 465:145–151.

687 Tyzio R, Holmes GL, Ben-Ari Y, Khazipov R (2007) Timing of the developmental switch in GABAA mediated signaling from
688 excitation to inhibition in CA3 rat hippocampus using gramicidin perforated patch and extracellular recordings.
689 Epilepsia 48:96–105.

690 Uwera J, Nedergaard S, Andreasen M (2015) A novel mechanism for the anticonvulsant effect of furosemide in rat
691 hippocampus in vitro. Brain Res 1625:1–8.

692 van Rheede JJ, Richards BA, Akerman CJ (2015) Sensory-Evoked Spiking Behavior Emerges via an Experience-Dependent
693 Plasticity Mechanism. Neuron 87:1050–1062.

694 Viitanen T, Ruusuvuori E, Kaila K, Voipio J (2010) The K+-Cl- cotransporter KCC2 promotes GABAergic excitation in the
695 mature rat hippocampus. J Physiol 588:1527–1540.

696 Wang BS, Feng L, Liu M, Liu X, Cang J (2013) Environmental Enrichment Rescues Binocular Matching of Orientation
697 Preference in Mice that Have a Precocious Critical Period. Neuron 80:198–209.

698 Wang DD, Kriegstein AR (2008) GABA Regulates Excitatory Synapse Formation in the Neocortex via NMDA Receptor
699 Activation. J Neurosci 28:5547–5558.

700 Wang DD, Kriegstein AR (2011) Blocking early GABA depolarization with bumetanide results in permanent alterations in
701 cortical circuits and sensorimotor gating deficits. Cereb Cortex 21:574–587.

702 Wierenga CJ, Müllner FE, Rinke I, Keck T, Stein V, Bonhoeffer T (2010) Molecular and electrophysiological characterization
703 of GFP-expressing ca1 interneurons in GAD65-GFP mice. PLoS ONE 5:1–11.

704 Wright R, Newey SE, Ilie A, Wefelmeyer W, Raimondo J V., Ginham R, Mcllhinney RAJ, Akerman CJ (2017) Neuronal
705 Chloride Regulation via KCC2 Is Modulated through a $GABA_B$ Receptor Protein Complex. J Neurosci 37:5447–
706 5462.

707 Yamada J, Okabe A, Toyoda H, Kilb W, Luhmann H, Fukuda A (2004) Cl− uptake promoting depolarizing GABA actions in
708 immature rat neocortical neurones is mediated by NKCC1. J Physiol 557:829–841.

709

710

711 ## Figure legends

712 **Figure 1**. ***Furosemide acutely depolarizes the GABAergic driving force, but results in hyperpolarization after***
713 ***one week treatment.***

714 A, B) GABA reversal potential (E_{GABA}) (PT, p=0.33) and GABA Driving Force (GABA DF) (PT, p=0.19) values recorded
715 in CA1 pyramidal cells at DIV2 before and after acute application of furosemide. Data from 4 cells, 4 slices and 4
716 mice.

717 C, D) E_{GABA} (MW, p=0.004) and GABA DF (MW, p=0.002) values recorded in CA1 pyramidal cells at DIV21 before
718 and after acute application of furosemide. Data from 6 cells, 6 slices and 5 mice.

719 E) Perforated patch-clamp recording in CA1 pyramidal cells in furosemide-treated and control slices at DIV9.
720 Responses to muscimol application were recorded at holding potentials from -100 mV to -30 mV with 10 mV
721 increments. The GABA reversal potential was determined from the intersection of the linear current-voltage
722 curve with the x-axis.

723 F,G) E_{GABA} (MW, p=0.001) and GABA DF (MW, p=0.005) recorded in CA1 pyramidal cells at DIV9 in control (CTL)
724 and furosemide-treated slices. Data from 7-9 cells, 5-8 slices and 4-5 mice per group.

725 H) Average SClm FRET ratios in CTL and furosemide-treated slice cultures (UT, p=0.75). Data from 10-14 slices
726 and 6-10 mice per group.

727 I) Cumulative distribution of FRET ratios in individual cells in CTL and furosemide -treated cultures. (KS, p=0.23).
728 Data from 15 randomly selected cells per slice.

729 J) Lower panel: Western blots of NKCC1, KCC2 and S940-pKCC2 (pKCC2) protein levels in CTL and furosemide-
730 treated slice cultures. Tubulin (Tub) was used as loading control.

731 K) Summary of data for NKCC1, KCC2 and for s940-pKCC2 (pKCC2) protein levels. Values were normalized to the
732 protein level in CTL cultures (NKCC1: MW, p>0.99; KCC2: MW, p=0.70; pKCC2: MW, p=0.48). Data from 3-5
733 experiments and 3 mice per group.

734 L) Confocal images of NeuN and KCC2 staining in CTL and furosemide-treated cultures. Yellow lines indicate the
735 outlines of individual cells. Scale bar: 10 µm.

736 M) Total KCC2 levels (UT, p=0.55) and KCC2 levels in membrane (UT, p=0.37) in CTL and furosemide-treated
737 cultures. Each datapoint represents the mean KCC2 intensity of all neurons in one image. Data from 8-17 images,
738 4-8 slices and 3 mice per group.

739

740 **Figure 2.** ***Furosemide does not affect inhibitory transmission at DIV9.***

741 A-E) sIPSC frequency (MW, p=0.084), amplitude (UT, p=0.83), risetime (MW, p=0.80) and decay tau (MW,
742 p=0.57) and membrane capacitance (Cm) (UT, p=0.63) in control (CTL) and furosemide-treated slice cultures at
743 DIV9. Data from 14-17 cells, 9 slices and 9 mice per group.

744 F-I) sIPSC frequency after ACSF wash in as a control CTL (WSR, p=0.008) and furosemide-treated (WSR, p=0.002)
745 slice cultures at DIV9. sIPSC frequency after TTX wash in of in CTL (WSR, p=0.80) and furosemide-treated WSR,
746 p=0.002) slice cultures at DIV9. Data from 8-15 cells, 8-15 slices and 7-10 mice per group.

747 J) Change in sIPSC frequency after ACSF wash in as a control, versus after wash in of TTX, K252a, AM251 and
748 agatoxin-IVA (aga) to block neuronal activity, BDNF, endocannabinoids and P/Q calcium channels respectively in
749 control and furosemide-treated slices at DIV9 (2W ANOVA, treatment p=0.18, blocker p=0.002; SMC, control
750 versus TTX, p=0.95; control versus K252a, p=0.020; control versus AM251, p=0.99; control versus agatoxin-IVA
751 (aga), p=0.82). Data from 7-15 cells, 7-15 slices and 4-10 mice per group.

752 **Figure 3.** ***Furosemide increases inhibitory transmission at DIV21.***

753 A,B) GABA reversal potential (E_{GABA}) (MW, p=0.56) and GABA Driving Force (GABA DF) (MW, p=0.76) in control
754 (CTL) and furosemide-treated slice cultures at DIV21. Data from 9-13 cells, 9 slices and 9 mice per group.
755 C) sIPSC recording from CA1 pyramidal cells in CTL and furosemide-treated organotypic cultures at DIV21. sIPSCs
756 are indicated with *.
757 D-G) sIPSC frequency (UT, p=0.10), amplitude (UT, p=0.034), risetime (UT, p=0.54) and decay tau (UT, p=0.34) in
758 CTL and furosemide-treated slice cultures at DIV21.
759 I) Membrane capacitance (Cm) of CA1 pyramidal cells in CTL and furosemide-treated slice cultures at DIV21 (UT,
760 p=0.035).
761 I) mIPSC recording from CA1 pyramidal cells in control and furosemide-treated organotypic cultures at DIV21.
762 mIPSCs are indicated with *.
763 J-M) mIPSC frequency (UT, p=0.0002), amplitude (UT, p=0.34), risetime (MW, p=0.73) and decay tau (UT, p=0.06)
764 in CTL and furosemide-treated organotypic cultures at DIV21.
765 N) Membrane capacitance (Cm) of CA1 pyramidal cells in the presence of TTX in CTL and furosemide-treated
766 slice cultures at DIV21 (UT, p=0.35). Data in D-H from 11-12 cells, 5-6 slices and 3-5 mice per group; data in J-N
767 from 12-13 cells, 5 slices and 4 mice per group.
768

769 **Figure 4.** ***Furosemide does not affect inhibitory synapses at DIV9.***

770 A,B) VGAT, PV and CB1R immunofluorescence in the CA1 *stratum Pyramidale* (*sPyr)* and *stratum Radiatum*
771 (*sRad)* of control (CTL) and furosemide-treated organotypic cultures at DIV9. Scale bar=10 µm.
772 C,D) The density (UT, p=0.50) and size (UT, p=0.47) of VGAT puncta in the *sPyr* of CTL and furosemide-treated
773 organotypic cultures at DIV9.
774 E,F) The density (UT, p=0.59) and size (UT, p=0.46) of VGAT puncta in *sRad* of CTL and furosemide-treated
775 organotypic cultures at DIV9.
776 G,H) The density of CB1R-positive VGAT puncta (UT, p=0.43) and PV positive VGAT puncta (UT, p=0.82) in *sPyr*
777 of CTL and furosemide-treated organotypic cultures at DIV9.
778 I) The density of CB1R-positive VGAT puncta (UT, p=0.68) in *sRad* of CTL and furosemide-treated organotypic
779 cultures at DIV9.
780 Data in C-I from 11-12 images, 6 slices and 2 mice per group.
781

782 **Figure 5.** ***Furosemide increases the number of VGAT puncta at DIV21 in sRad.***

783 A,B) VGAT, PV and CB1R immunofluorescence in the CA1 *stratum Pyramidale* (*sPyr)* and *stratum Radiatum*
784 (*sRad)* of control (CTL) and furosemide-treated organotypic cultures at DIV21. Scale bar=10 µm.

785 C,D) The density (UT, p=0.09) and size (UT, p=0.14) of VGAT puncta in *sPyr* of CTL and furosemide-treated
786 organotypic cultures at DIV21. Data from 16 images, 8 slices and 3 mice per group.
787 E,F) The density (MW, p=0.019) and size (MW, p=0.015) of VGAT puncta in *SRad* of CTL and furosemide-treated
788 organotypic cultures at DIV21. Data from 13 images, 7 slices and 3 mice per group.
789 G,H) The density of CB1R (UT, p=0.11) and PV positive VGAT puncta (UT, p=0.89) in *sPyr* of CTL and furosemide-
790 treated organotypic cultures at DIV21. Data from 16 images, 8 slices and 3 mice per group.
791 I) The density of CB1R-positive VGAT puncta (MW, p=0.30) in *SRad* of CTL and furosemide-treated organotypic
792 cultures at DIV21. Data from 13 images, 7 slices and 3 mice per group.

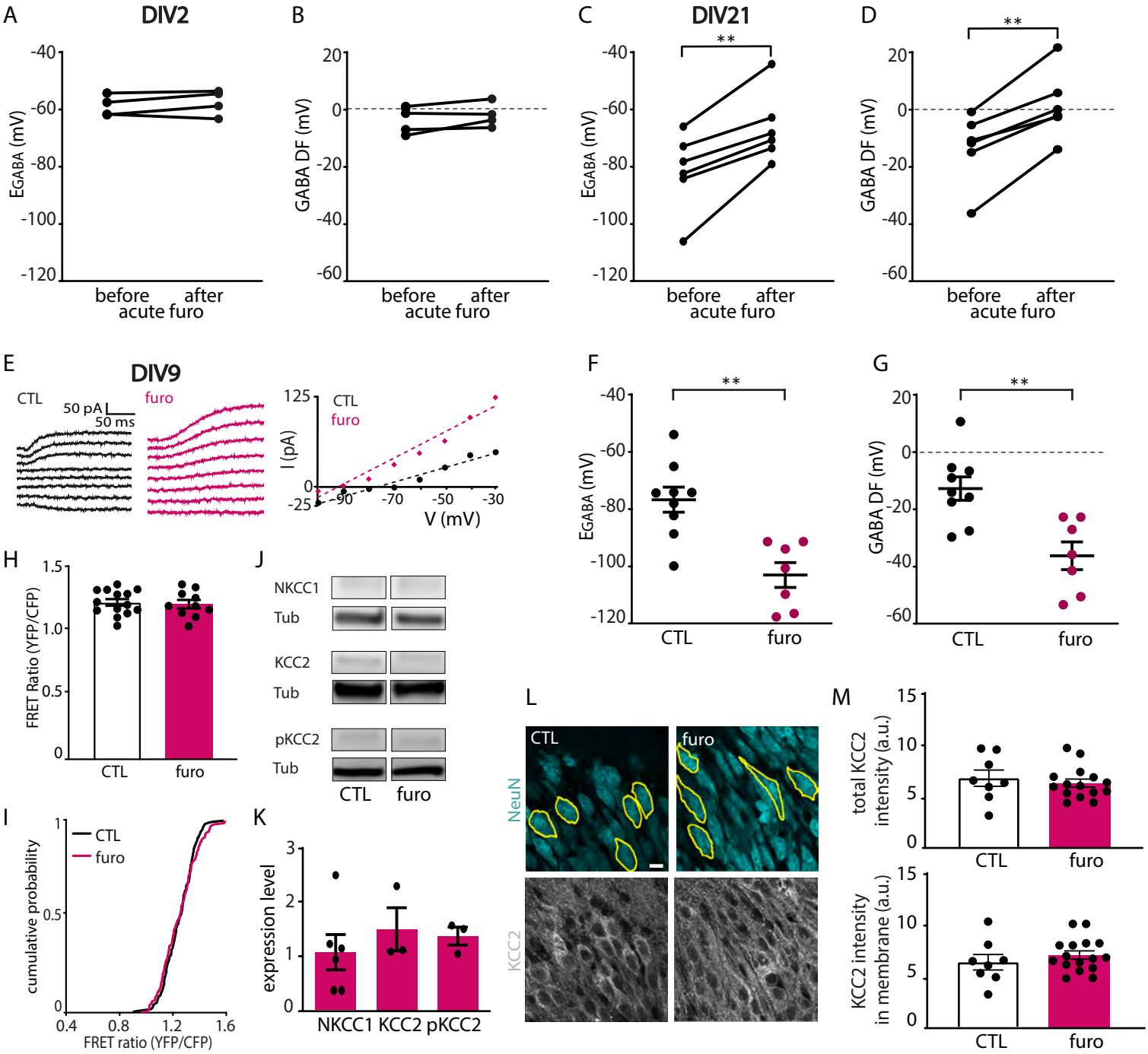

Peerboom et al. - Figure 1

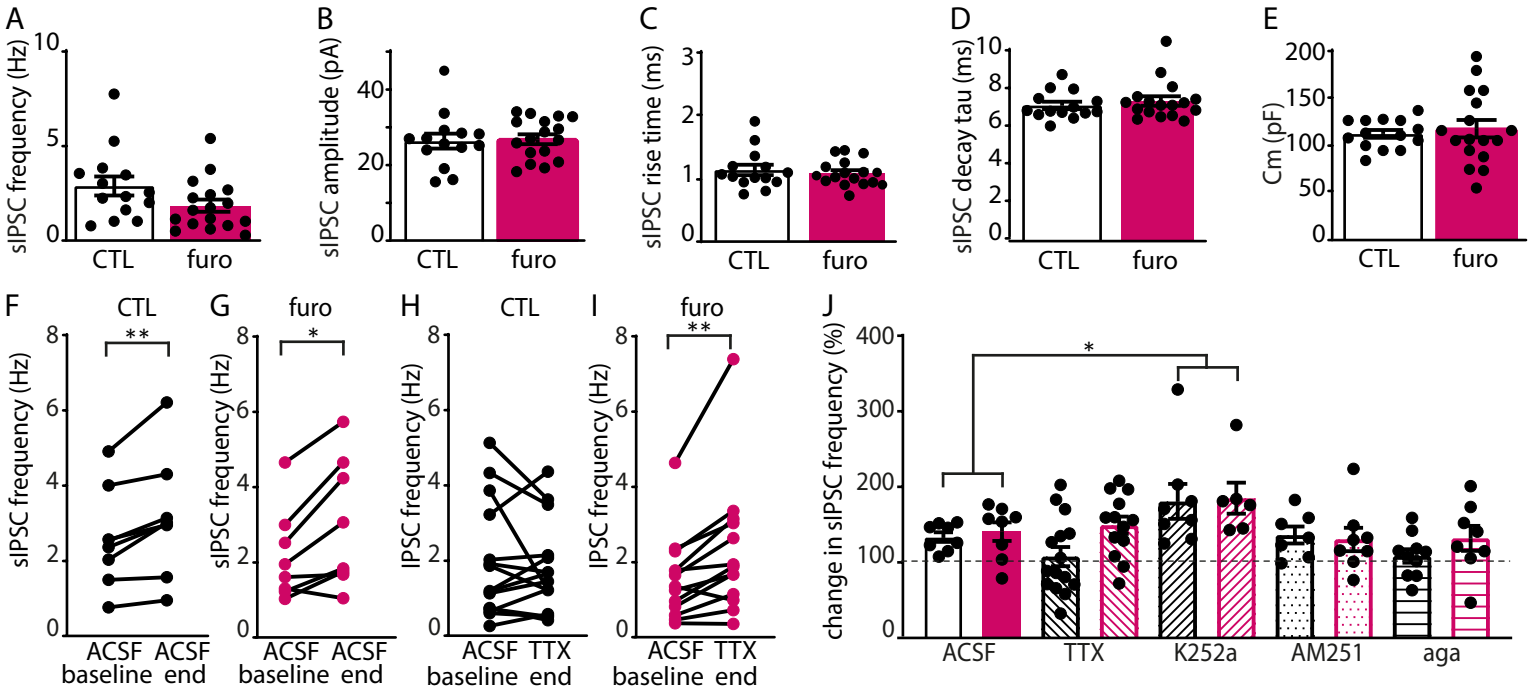

Peerboom et al. - Figure 2

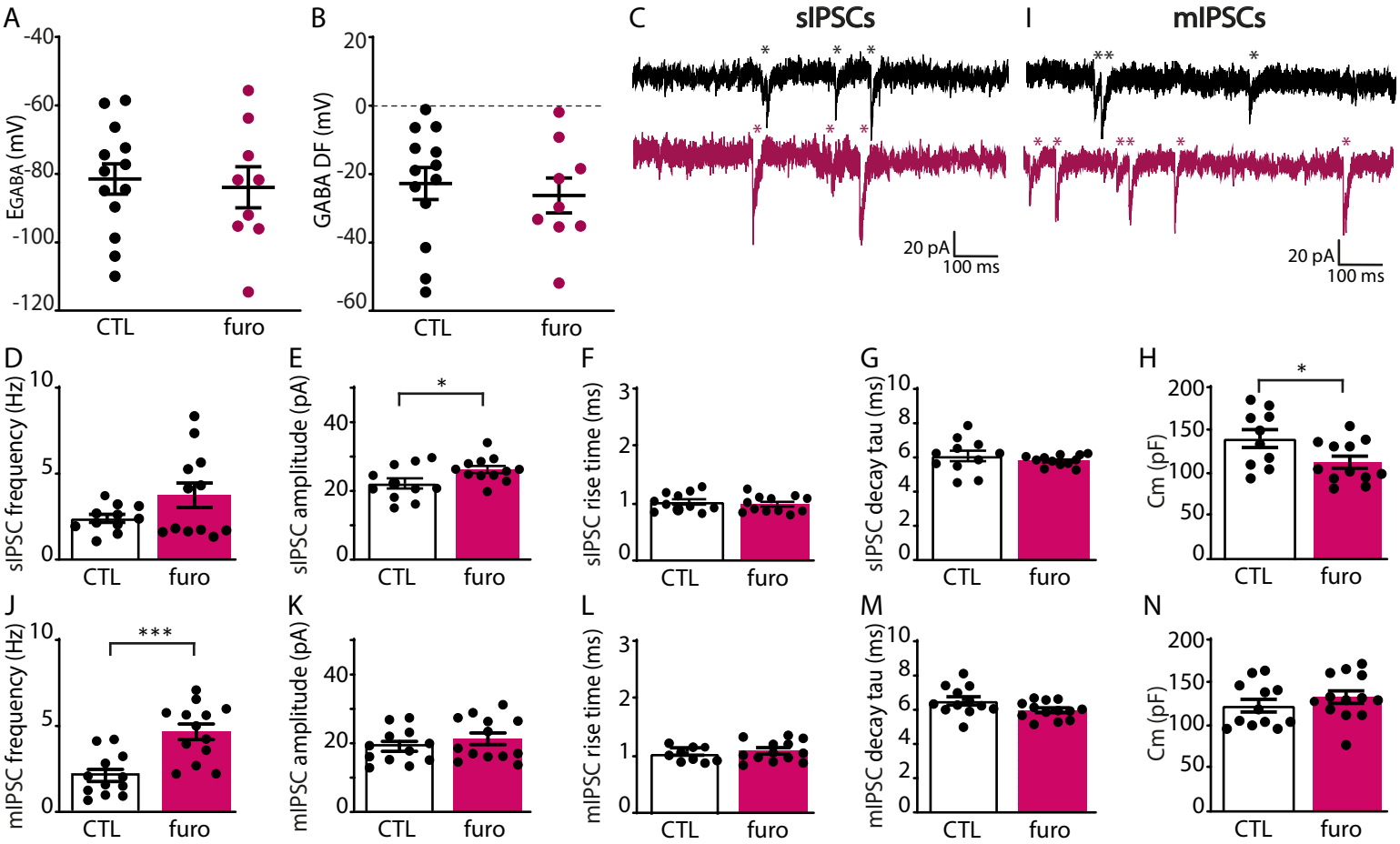

Peerboom et al. - Figure 3

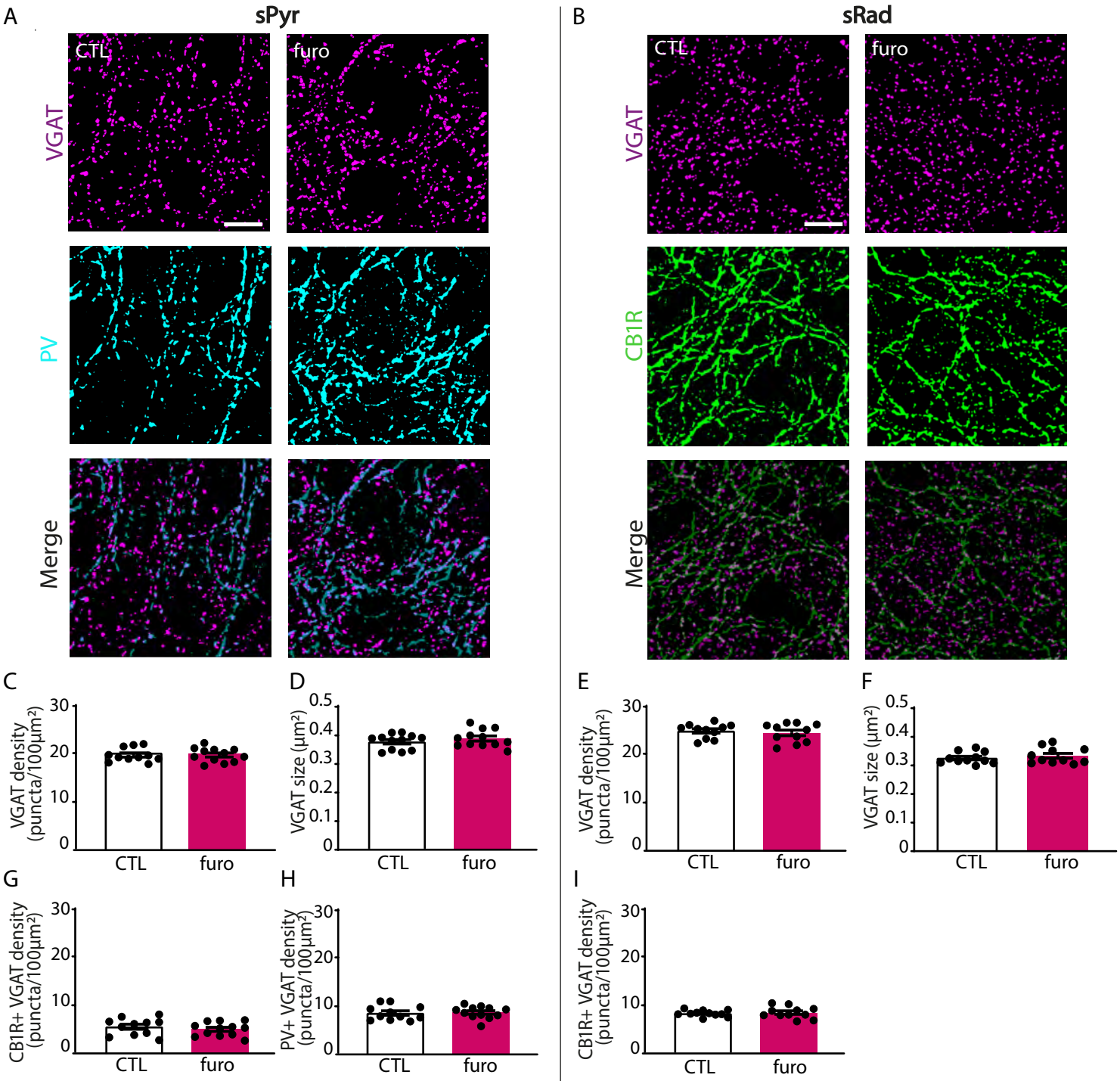

Peerboom et al. - Figure 4

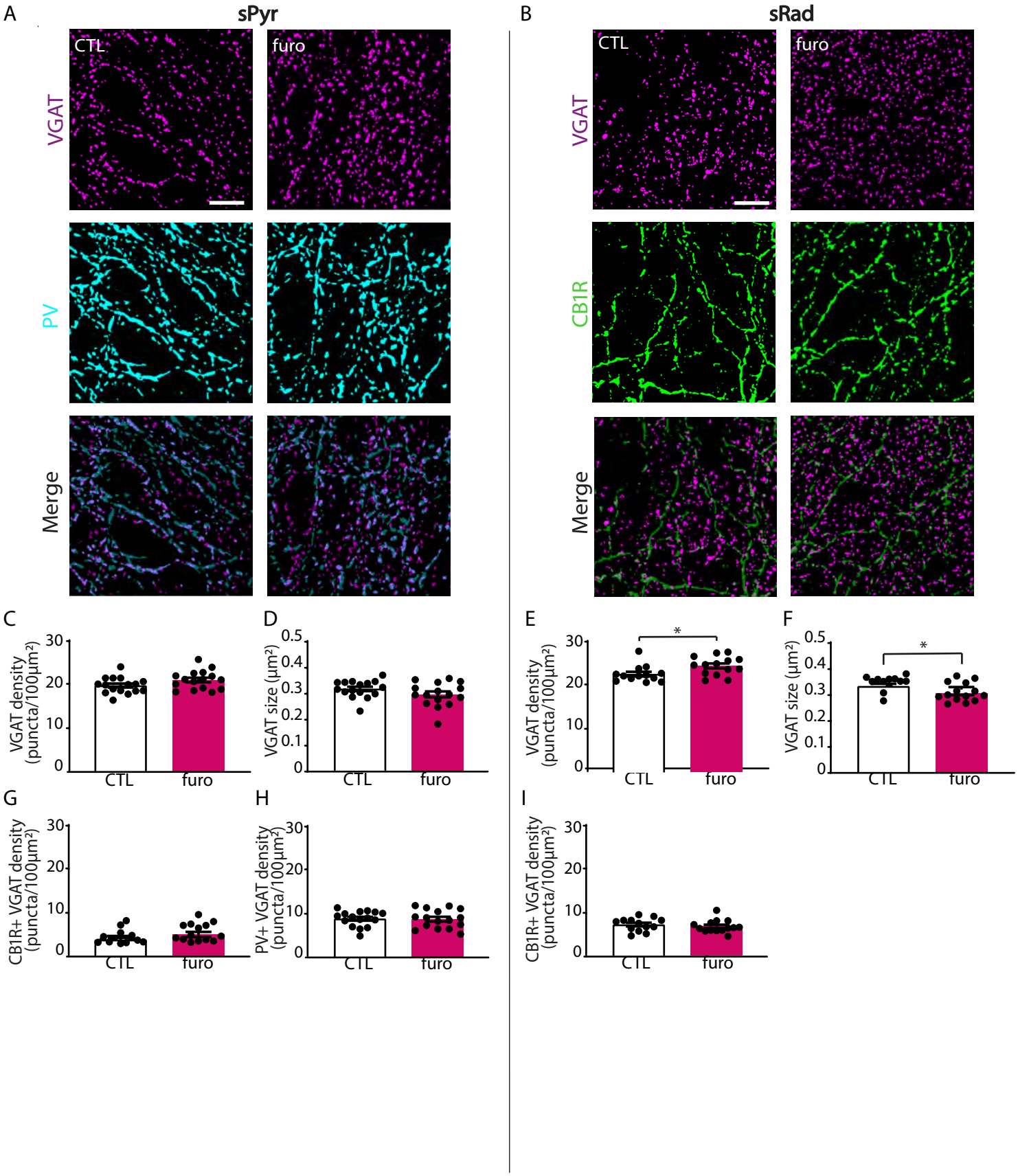

Peerboom et al. - Figure 5

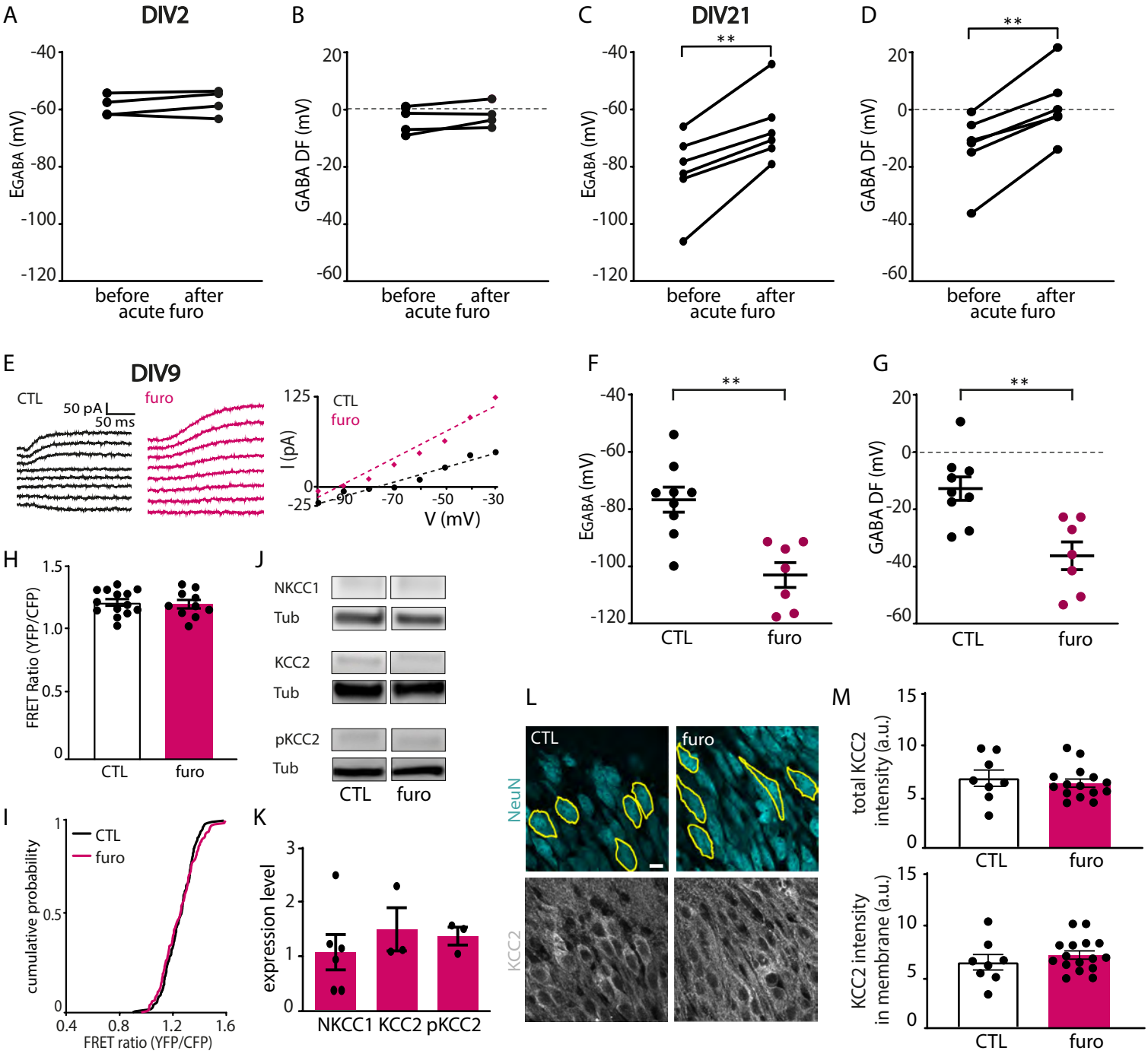

Peerboom et al. - Figure 1

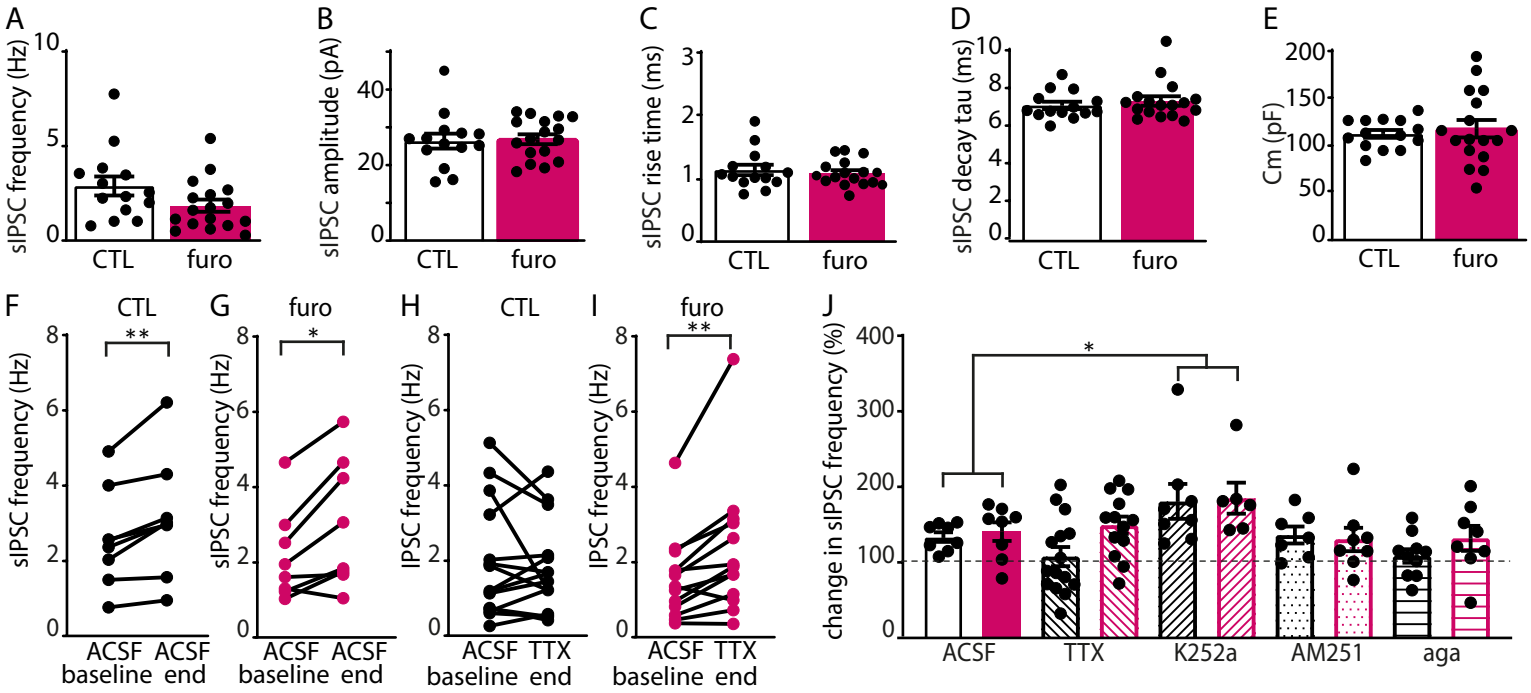

Peerboom et al. - Figure 2

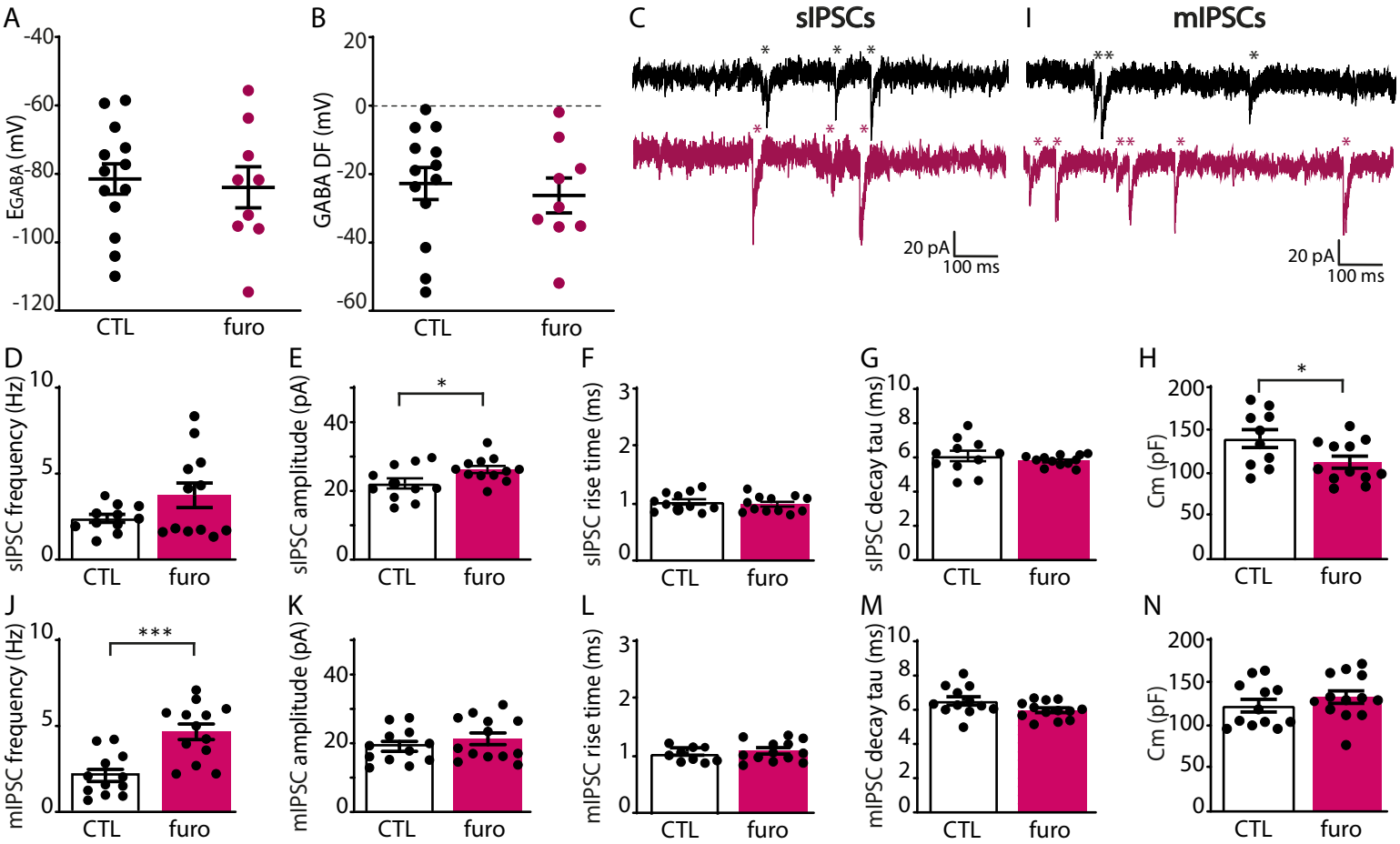

Peerboom et al. - Figure 3

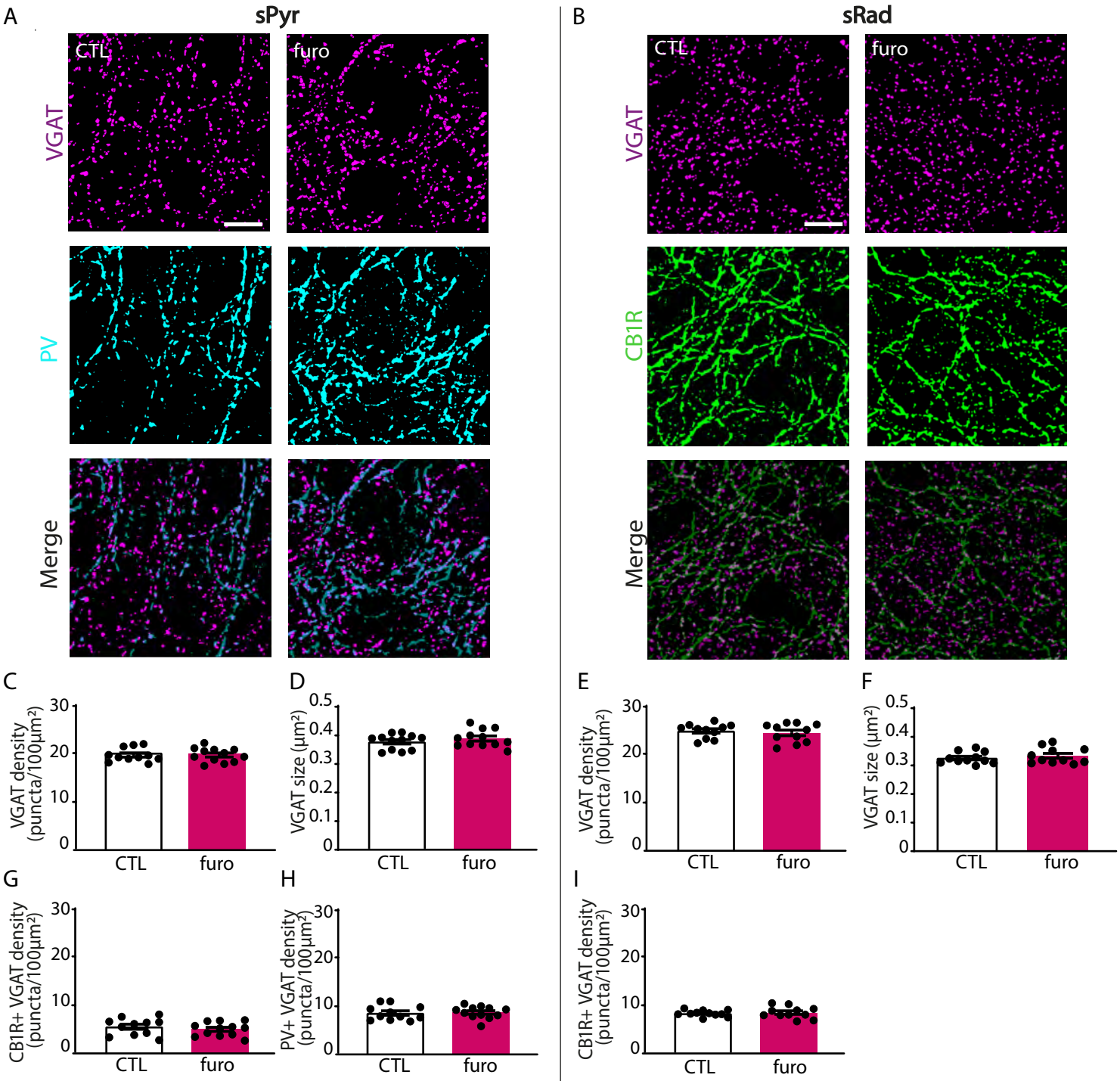

Peerboom et al. - Figure 4

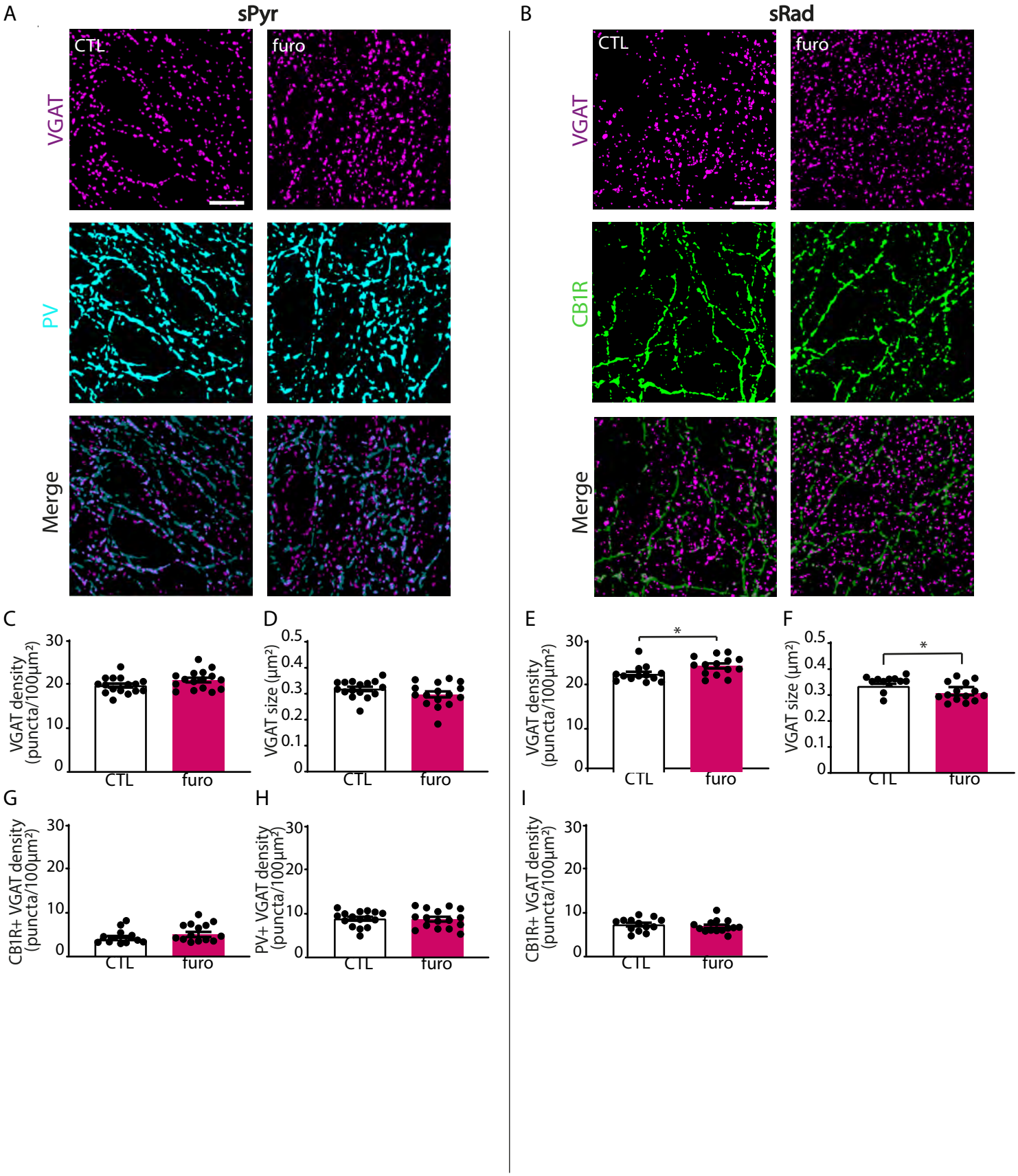

Peerboom et al. - Figure 5